A new model for the global biogeochemical cycle of carbonyl sulfide. Part 1: Assessment of direct marine emissions with an oceanic general circulation and biogeochemistry model

T. Launois[1], S. Belviso[1], L. Bopp[1], C.G. Fichot[2] and P. Peylin[1]

[1] Laboratoire des Sciences du Climat et de l'Environnement (LSCE Saclay), IPSL, CEA, CNRS, UVSQ, CE Saclay, Bât 703 L'Orme des Merisiers, 91191, Gif-sur-Yvette, France

[2] Jet Propulsion Laboratory, California Institute of Technology, Pasadena, California, USA

Correspondence to: T. Launois (thomas.launois@lsce.ipsl.fr)

Abstract

The global budget of tropospheric carbonyl sulfide (OCS) is believed to be at equilibrium because background air concentrations have remained roughly stable over at least the last decade. Since the uptake of OCS by leaves (associated to photosynthesis) and soils have been revised significantly upwards recently, an equilibrated budget can only be obtained with a compensatory source of OCS. It has been assumed that the missing source of OCS comes from the low-latitude ocean, following the incident solar flux. The present work uses parameterizations of major production and removal processes of organic compounds in the NEMO-PISCES Ocean General Circulation and Biogeochemistry Model to assess the marine source of OCS. In addition, the OCS photo-production rates computed with the NEMO-PISCES model were evaluated independently using the UV absorption coefficient of chromophoric dissolved organic matter (derived from satellite ocean color) and apparent quantum yields available in the literature. Our simulations show global direct marine emissions of OCS in the range of 573-3997 GgS yr^{-1}, depending mostly on the quantification of the absorption rate of chromophoric dissolved organic matter. The high estimates on that range are unlikely, as they correspond to a formulation that most likely overestimate photo-production process. Low and medium (813 GgS yr-1) estimates derived from the NEMO-PISCES model are however consistent spatially and temporally with the suggested missing source of Berry et al. (2013), allowing thus to close the global budget of OCS given the recent estimates of leaf and soil OCS uptake.

1 Introduction

Carbonyl sulfide (OCS) is a long-lived sulfur-containing trace gas with direct and indirect effects on the radiation budget of the atmosphere (OCS being both a tropospheric greenhouse gas and a source of sulfur aerosols to the stratosphere). But these radiative effects are low compared to the radiative forcings of greenhouse gases (GHG) and tropospheric aerosols of anthropogenic origin (Brühl et al., 2012 and references therein). But because OCS is the most abundant sulfur-containing gas in the atmosphere, it is a major contributor to the stratospheric sulfate layer during volcanically quiescent periods (Notholt et al., 2003). OCS also participates in some key reactions within the global carbon cycle, especially reactions associated with leaf photosynthesis and soil microbial activities (Berry et al., 2013 and references therein). As such, it holds great promises for the studies of plant physiology, terrestrial ecosystem production and the global carbon cycle thanks to its potential use as a tracer for canopy photosynthesis, transpiration and stomatal conductance (Wohlfahrt et al., 2012 and references therein).

Measurements of OCS from the global air-monitoring network of the National Oceanic and Atmospheric Administration (NOAA) provided compelling evidence for the existence of a major sink of this gas in the continental boundary layer, mainly attributed to biospheric uptake (Montzka et al., 2007; Campbell et al., 2008). The uptake of OCS by plants was modeled to be no more than 240 GgS yr^{-1} by Kettle et al. (2002), but it has been recently revised upwards, with new estimates of 490 GgS yr^{-1} (Suntharalingam et al., 2008), of 738 GgS yr^{-1} in the work of Berry et al. (2013) and even reaching up to 1500 GgS yr^{-1} in Montzka et al. (2007). Soils could also play a role in the budget of OCS. It is still a strong matter of debate but recent estimates suggest that much more OCS is taken up by soils than proposed by Kettle et al. (2002) (355 GgS yr^{-1}, according to Berry et al., 2013, compared with an estimate of around 130 GgS yr^{-1} in Kettle et al., 2002). Since background air concentrations have remained roughly stable over at least the last decade (Montzka et al., 2007), the global budget of tropospheric OCS is believed to be at equilibrium. Kettle et al. (2002) proposed a global budget of OCS with ocean and anthropogenic sources compensating for the main uptake by vegetation. However, because deposition fluxes of OCS to vegetation and soils are three times higher than proposed in the study by Kettle et al. (2002), an equilibrated budget can only be obtained with a compensatory source of OCS. Berry et al. (2013) suggests that the missing source of OCS comes from the oceans. This missing source has been inferred through a simple inversion approach that optimizes sources and sinks based on global measurements of

atmospheric OCS mixing ratios collected in the NOAA network. This inversion pointed towards a larger global oceanic source of OCS with higher proportions of tropical emissions than previously established.

The ocean is believed to be the largest source of atmospheric OCS (Chin and Davis, 1993; Kettle et al., 2002; Berry et al., 2013). It contributes to OCS in the troposphere by direct emission of this gas, and by large emissions of carbon disulfide (CS_2) and dimethylsulfide (DMS) quickly oxidized into OCS (with an approximate lifetime of 1 day) (Barnes et al., 1994; Kloster, 2006). Barnes et al. (1994) suggested that OCS accounts for 0.7% of the oxidation products of DMS, and that 87% of the marine emissions of CS_2 are converted into OCS. However, estimates of sea-air fluxes of OCS and their spatial distributions remain largely unknown. Kettle et al. (2002) simulated direct global oceanic OCS fluxes from -110 GgS yr^{-1} (a sink) to 190 GgS yr^{-1} (a source to the atmosphere), while previous estimates based on field observations suggested global direct oceanic OCS emissions from 160 to 640 GgS yr^{-1} (Chin and Davis, 1993; Watts, 2000). The Kettle et al. (2002) study suggested that direct sea-air OCS emissions mainly take place at mid and high latitudes, during the respective periods of maximum irradiance.

OCS surface concentrations show a strong diurnal cycle with a mid-afternoon maximum, suggesting that photo-production is a major source of marine OCS (Ferek and Andreae, 1984; Xu et al., 2001; Von Hobe et al., 2003). In addition, OCS can also be produced in marine waters when no light is available. This pathway is therefore called dark-production. Measurements by Von Hobe et al. (2001) indicated that its rate is proportional to the amount of organic material, and it has therefore so far been linked to the chromophoric dissolved organic matter (CDOM) absorption coefficient (Von Hobe et al., 2001 and 2003). Finally, OCS surface concentrations and fluxes are also strongly influenced by the continuous temperature- and pH-dependent hydrolysis of OCS to carbon dioxide (CO_2) and hydrogen sulfide (H_2S) (Von Hobe et al., 2003).

The present work reassesses the marine source of OCS using the 3D oceanic NEMO-PISCES Ocean General Circulation and Biogeochemistry model with process-based parameterizations of the main OCS production and removal processes (Fig. 1). The present study proposes two independent approaches to quantify the photo-production of OCS. The dark-production rate implemented in the NEMO-PISCES model follows the formulation of Von Hobe et al. (2001, 2003). Therefore, the dark-production rate, even if supposed to be light-independent, is also linked to the chromophoric dissolved organic matter absorption coefficient at 350nm (a_{350}), as

the variable provides an indirect estimate of the seawater richness in organic matter. As parameterizations found in literature for both dark- and photo-production of OCS are related to the UV absorption coefficient of CDOM at 350 nm, sensitivity tests are performed using three different formulations for this variable. Sensitivity tests are also performed on hydrolysis, exploring two different formulations. Global maps of OCS concentrations obtained with the NEMO-PISCES model are compared with in-situ measurements. Finally, the magnitude and spatial distributions of global OCS emissions modeled in the present work are compared to previous global estimates.

2 Methods

2.1 Description of NEMO-PISCES and experimental design

In this study, we use the Pelagic Interaction Scheme for Carbon and Ecosystem Studies (PISCES) ocean biogeochemical model. As a detailed description of the model parameterizations is given in Aumont and Bopp (2006), the model is only briefly presented here. The model has 24 compartments, including four living pools: two phytoplankton size classes/groups (nanophytoplankton and diatoms) and two zooplankton size classes (microzooplankton and mesozooplankton). Phytoplankton growth can be limited by five different nutrients: nitrate, ammonium, phosphate, silicate and iron. The internal concentrations of chlorophyll for both phytoplankton groups are prognostically simulated with Chlorophyll-to-Carbon ratios computed as a function of light and nutrient stress. There are three nonliving compartments: semi-labile dissolved organic matter (with remineralization timescales of several weeks to several years), small and large sinking particles. In addition to the version of the model used in Aumont and Bopp (2006), we also include here a prognostic module computing OCS concentrations in seawater.

PISCES is coupled to the general circulation model Nucleus for European Modelling of the Ocean (NEMO, Madec et al. 1998). A release of the model is available for the community (http://www.nemo-ocean.eu/). Here, we use the global configuration ORCA2 with a resolution of 2° x 0.5-2° and 31 vertical levels (with a ~10m-resolution in the first 200m). NEMO-PISCES is first run 3,000 years to obtain an equilibrated state, forced in offline mode by the Consortium for Oceanic Research and Education (CORE2) Normal Year Forcing, (Large and Yeager (2008)) and initialized with climatological nutrient data. The OCS module is then only run two additional years as it converges towards equilibrium much more rapidly. The results presented in this study correspond to the last year of this simulation.

2.2 Parameterizations of OCS production and removal processes implemented in NEMO-PISCES

The clear diurnal cycle of sea-surface OCS concentrations with peak values during mid-afternoon suggests photochemical processes play an important role in the production of OCS. Organo-sulfur compounds with thiol groups (-SH), such as cysteine and methyl mercaptans (CH_3SH), have been suggested as OCS precursors (Ferek and Andreae, 1984; Flöck et al., 1997; Ulshöfer et al., 1996). Moreover, measured CH_3SH diurnal cycles were coherent with the hypothesis that its photo-destruction could lead to OCS production (Xu et al., 2001). Because no global map of CH_3SH is available, we followed parameterizations of OCS photo-production found in literature which relate photo-production rate of OCS to the UV irradiance intensity at the sea surface and to the efficiency of chromophoric dissolved organic matter (CDOM) available to absorb this UV radiation. The quantification of this photochemical process can be amenable to remote sensing because of its critical dependence on ocean UV and visible optical properties. Additional parameterizations were needed to complete the description of OCS formation and destruction processes in NEMO-PISCES. We therefore implemented specific equations to calculate the formation of OCS via dark-production (a light-independent pathway) and the hydrolysis rate of OCS in sea waters. Finally, air-sea exchanges of OCS were described in an analogous way to Fick's diffusion law.

2.2.1 UV light penetration in seawater:

In NEMO-PISCES, surface irradiance received at each grid point is a function of cloud coverage and deduced surface UV irradiance is taken equal to 4.4% of the total light received at sea surface. UV penetration at depth in marine waters in NEMO-PISCES was taken equal to the penetration calculated with the deep blue wavelength for visible light attenuation coefficient. As this is a rough approximation and might lead to over-estimating maximum depth penetration for UV irradiance, we set the UV value to zero for layers deeper than 30 m, which corresponds to the average depth at which less than 10% of surface UV irradiance penetrates for marine waters containing less than $1mg\ m^{-3}$ of chlorophyll (Bricaud et al., 1995; Tedetti et al., 2007).

2.2.2 Parameterization of CDOM absorption coefficient at 350 nm (a_{350})

Chromophoric (or colored) dissolved organic matter (CDOM) is the fraction of the dissolved organic matter that absorbs light, ranging from ultraviolet to visible wavelengths. CDOM has been identified as one of the most influential factors to control UV attenuation in waters. Its concentration increases in seawater with elevated biological production rates and terrestrial

inputs. CDOM distribution is also controlled by the deep ocean circulation, upwelling and/or vertical mixing (Para et al., 2010 and references therein). Its concentration decreases with photochemical degradation and microbial consumption. CDOM absorbs part of available light, therefore negatively impacting primary productivity of aquatic ecosystems. However, as provider of a substitute for microbial respiration, photo-degraded CDOM positively impacts the secondary productivity of the oceanic ecosystems.

As no reliable parameterization is currently available to calculate CDOM concentrations, due to insufficient knowledge on the controlling processes of CDOM formation and destruction, we chose to follow the study from Para et al. (2010) and assumed that the CDOM absorption at 350nm (a_{350}) was a good indicator of CDOM concentrations. The wavelength of 350nm was chosen because it corresponds to the maximum sensitivity of the Eppley UV light sensors used during the marine campaigns where links between CDOM concentration, CDOM absorption and OCS production were established (Uher et al., 1997; Preiswerk et al., 2000). This wavelength has also been proven to be the most efficient for the photochemical excitation of dissolved organic matter (Farmer et al., 1993). OCS production is either dependent on irradiance in the UV domain (photo-production) or on CDOM and organic matter concentration (dark-production). As a_{350} allows a link with both variables, it is a key parameter in our parameterizations of OCS production. Sensitivity tests were performed using NEMO-PISCES and three different formulations of a_{350}.

The first two formulations of CDOM absorption coefficients were proposed by Morel and Gentili (2009) and Preiswerk et al. (2000), who deduced them at a given wavelength from in situ measurements, and then extrapolated the absorption coefficient of CDOM at 350 nm by using the following standard exponential relation:

$$a_{CDOM}(\lambda) = a_{CDOM}(\text{ref}) * e^{\left(-S*(\text{ref}-\lambda)\right)} \qquad (1)$$

where S is the spectral slope coefficient of CDOM between λ and the reference wavelength (ref).

a) a_{350} from Morel and Gentili (2009)

The parameterization of a_{350} from Morel and Gentili (2009) is based on spectral reflectances of the ocean over Case 1 waters. Case 1 waters are those for which the optical properties of CDOM closely follow the optical properties of phytoplankton, as defined in Morel (1988). Spectral reflectances were derived from ocean color remote sensing data at several wavelengths to allow separation between CDOM and chlorophyll reflectance signatures.

Products from SeaWiFS monthly global composites for the 2002-2007 period were used, and led to the following relation between CDOM absorption coefficient and chlorophyll concentration:

$$a_{CDOM}(400) = 0.065[\text{Chl}]^{0.63} \qquad (2)$$

b) a$_{350}$ from Preiswerk et al. (2000)

The second parameterization was taken from Preiswerk et al. (2000) who deduced a$_{350}$ from modeled CDOM absorption coefficient at 440 nm. To model a$_{440}$, satellite ocean color data were used as a proxy for chlorophyll concentration and combined with the relation of Garver and Siegel (1998), Eq. (3):

$$\text{per}(a_{440}) = -26\,[\log(\text{chl})] + 26 \qquad (3)$$

$$a_{PH,440} = 0.0448\text{chl} \qquad (4)$$

$$\text{per}(a_{440}) = \frac{a440}{aPH,440 + a440} * 100\% \qquad (5)$$

where $a_{PH,440}$ is the absorption coefficient of the phytoplankton at 440 nm, and $\text{per}(a_{440})$ is the percent of the total non-seawater absorption coefficient at 440 nm (due to CDOM).

c) a$_{350}$ from MODIS *Aqua* ocean color

A relationship between a_{350} and chlorophyll-a was established independently, using MODIS *Aqua* ocean color data collected continuously between July 2002 and July 2010. Monthly climatologies of MODIS *Aqua* chlorophyll-a surface concentrations were used, and MODIS *Aqua* remote-sensing reflectances were used to derive corresponding monthly climatologies of a_{350} for the global surface ocean. The Sea*UV* algorithm developed by Fichot et al. (2008) was used to estimate the diffuse attenuation coefficient at 320 nm, $K_d(320)$, from the remote-sensing reflectances. A ratio $a_{CDOM}(320)/K_d(320) = 0.68$ derived from an extensive set of in situ measurements was then used to calculate the absorption coefficient of CDOM at 320 nm, a_{320}, from $K_d(320)$ (Fichot and Miller, 2010). A spectral slope coefficient of 0.0198 derived from the same *in situ* data set was then used to calculate a_{350} from a_{320} using Eq. (1).

The a_{350} data from the twelve monthly climatologies were regressed on the corresponding MODIS *Aqua* chlorophyll-a concentrations using the fourth-order polynomial shown in Eq. (6).

$$\ln(a_{350}) = 0.5346C - 0.0263C^2 - 0.0036C^3 + 0.0012C^4 - 1.6340 \quad (6)$$

where C is the chlorophyll concentration in mg m^{-3}, and a_{350} has units of m^{-1}.

The equation 6 was then added in NEMO-PISCES to complete the sensitivity tests of the OCS concentrations on the different a$_{350}$ expressions tested.

2.2.3 OCS photo-production rates as modeled in NEMO-PISCES

OCS photo-production is primarily induced by the interaction of UV radiation and natural photosensitizers in CDOM (Ferek and Andreae, 1984; Flöck et al., 1997). Therefore, the Uher et al. (1997) photo-production parameterization takes into account both the incident UV irradiance and OCS production efficiency (apparent quantum yield, AQY). An AQY represents the spectral efficiency of a photochemical process (e.g., photochemical production of OCS), and is generally determined in the laboratory by normalizing the quantity of OCS produced during solar exposure to the amount of photons absorbed by CDOM during that same solar exposure. The resulting expression for photoproduction rate proposed is:

$$P = p \ UV \hspace{3cm} (7a)$$

where P is the OCS photo-production rate, p a zeroth-order photoproduction constant (fmol $L^{-1} s^{-1} W^{-1}$ m²) and UV the solar UV light density.

This expression was established using strong assumptions, such as considering that no other source or sink of OCS affects OCS concentration in seawaters. In their study, Uher et al. (1997) measured mean values for the photoproduction constant p around 1.3 ± 0.3 fmol $L^{-1} s^{-1}$ W^{-1} m² on offshore samples and values twice as high in inshore waters, around 2.8 ± 0.3 fmol $L^{-1} s^{-1} W^{-1}$ m² (all measurements done in April 1993, in the North Sea).

A few AQY for OCS have been published, but they exhibit considerable variability, with values varying by a factor of >7 depending on the environment considered (quantum yields ranging from $9.3 \cdot 10^{-8}$ to $6.4 \cdot 10^{-7}$ in the Sargasso Sea for Weiss et al., 1995a and Zepp et al., 1994, respectively). The quantum yields depend both on the location and the season of the measurement, especially because CDOM quality and its absorption coefficient might vary through time (Kettle et al., 2002; Weiss, 1995b; Cutter et al., 2004). To compensate for part of this natural variability, Uher et al. (1997) normalized the measured AQY by the absorption coefficient of CDOM available for the reaction at the same location. Therefore, the new relation, implemented in NEMO-PISCES, is the following:

$$P = a_{350} \ UV \ \frac{p}{a_{350}} = k \ a_{350} \ UV \hspace{2cm} (7b)$$

where P is the OCS photo-production rate (pmol $m^{-3} s^{-1}$), UV is the incident irradiance integrated from 295 to 385nm (W m^{-2}). The k coefficient is retrieved from the normalization of measured photoproduction constants to measured CDOM absorption coefficient values at 350 nm. For offshore waters (the majority of globe waters), k was found, in Uher et al. (1997) study, to be close to a value of 2.1 fmol $L^{-1} s^{-1} W^{-1}$ m^3. Note that the k coefficient deduced from inshore water samples was found to be 2.8 fmol $L^{-1} s^{-1} W^{-1}$ m^3 on average. The smaller

difference between the two k values justified the choice to use this normalized expression rather than Eq. 7a which showed more sample-dependence.

2.2.4 Parameterization of OCS dark-production rates

Measurements of large OCS concentrations well below the photic zones have proven that OCS can be produced when no light is available. The so-called dark-production pathway was shown to largely depend on available organic matter. The pool of organic matter is quantified by the a_{350} parameter, following Para et al. (2010), as explained in Section 2.2.2. Microbial activities are suggested as main precursors for the OCS dark-production pathway, but their exact nature and the mechanisms underlying this process are poorly known. Von Hobe et al. (2001, 2003) calculated dark-production rates assuming that after dawn OCS concentrations were reaching a steady-state when dark-production was compensating for the parallel hydrolysis. Equation 8 was established using measurements from a campaign in the Sargasso Sea and hydrolysis rates were calculated following the Elliott et al. formulation (1989).

The formulation from Von Hobe et al. (2001) relating OCS dark-production rates to the CDOM absorption coefficient was implemented in NEMO-PISCES following:

$$Q = a_{350}e^{(55.8-\frac{16200}{T})} \quad \text{(T in K)} \tag{8}$$

where Q is the dark-production rate in pmol m^{-3} s^{-1}, and a_{350} is the CDOM absorption coefficient which is used here to describe the CDOM/organic matter concentration.

2.2.5 Hydrolysis of OCS

OCS is chemically removed in seawater through reaction with H_2O and OH^-:

$$H_2O + OCS \leftrightarrow H_2S + CO_2 \tag{9a}$$

$$OH^- + OCS \leftrightarrow HS^- + CO_2 \tag{9b}$$
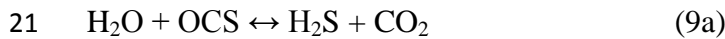
OCS hydrolysis rate measurements were done in the dark, using filtered water, therefore cancelling the potential impact of parallel dark-production. Reactions 9a and 9b are actually composites of complex mechanisms involving several intermediates, and concentrations that have been used to calculate hydrolysis rates are much larger than observed in seawater, which may lead to some errors.

We performed sensitivity tests in NEMO-PISCES by using two different hydrolysis parameterizations to study the impact of the choice of the hydrolysis constant formulation. Both Kamyshny et al. (2003) and Elliott et al. (1989) relate the value of OCS hydrolysis constant to the marine water pH and its temperature, following respectively:

$$k_{hydr\_Elliott} = e^{(24.3-\frac{10450}{T})} + \frac{kw}{[H+]}e^{(22.8-\frac{6040}{T})} \quad \text{(T in K)} \tag{10a}$$

1 $$k_{hydr\_Kamyshny} = 4.19E^{-12}e^{\left(-\frac{12110}{T}\right)} + \frac{kw}{[OH-]}1.41E^{18}e^{\left(-\frac{-11580}{T}\right)} \quad \text{(T in K)} \quad \text{(10b)}$$

2

3 With k_w the ion product of marine water, [OH-] and [H+] the OH- and H+ activities.

4 Both hydrolysis constant rates, as function of temperature, are represented in the case of

5 pH=8.2 in Fig. 2.

6 **2.2.6 OCS sea-to-air fluxes**

7 OCS exchange between the ocean and the atmosphere can be described in an analogous way

8 to Fick's diffusion law. The sea-air OCS flux depends on the OCS concentration in sea water

9 and the partial pressure of OCS in air:

10 $$F_{OCS} = k_{water}\left([OCS]_{aq} - \frac{[OCS]_{atm}}{H}\right) \quad \text{(11)}$$

11 where F_{OCS} is the sea-air flux (pmol m^{-2} s^{-1}), $[OCS]_{aq}$ and $[OCS]_{atm}$ are the OCS concentration

12 at sea surface and in the atmosphere respectively (in pmol m^{-3}). The atmospheric OCS

13 concentration $[OCS]_{atm}$ over sea surface was constantly imposed when running NEMO-

14 PISCES, assuming an atmospheric mixing ratio of 500 ppt. Through H, the Henry's law

15 constant, the sea-air OCS flux also depends on the air temperature, and was implemented in

16 NEMO-PISCES following the expression established by Johnson et al. (1986):

17 $$H = e^{\left(12722 - \frac{3496}{T}\right)} \quad \text{(T, air temperature in K)} \quad \text{(12)}$$

18 k_{water} is the piston velocity (in m.s^{-1}) for OCS. The coefficient is deduced from the Schmidt

19 number of OCS and depends on surface wind speed, and is calculated with the relation of

20 Wanninkhof (1992):

21 $$k_{water} = [0.3u^2 + 2.5*(0.5246 + 0.016256T + 0.00049946T^2)] * \sqrt{\frac{660}{S_{OCS}}} \quad \text{(T air}$$

22 temperature in °C) (13)

23 Where u is the wind speed (in m.s^{-1}).

24 Note that Kettle et al. (2002) used similar parameterizations for the sea-surface exchange

25 coefficient and the same relation from Wanninkhof et al. (1992) to model the global OCS flux

26 at sea surface to the one presented in this work.

1. The Schmidt number for OCS, S_{ocs}, dimensionless, was implemented in NEMO-PISCES

2. following the suggestion by Ulshöfer (1995) to deduce it from kinetic viscosity (v) and

3. diffusion coefficient (D) (both in $m^2.s^{-1}$), respectively derived from:

4. $$S_{OCS} = \frac{v}{D} \qquad (14)$$

5. with:

6. $$v = (1.792747 - 5.126103E^{-2}T + 5.918645E^{-4}T^2) * 1E^{-6} \quad \text{(T, air temperature in °C)}$$

7. (15)

8. $$D = \left(10^{\left(\frac{-1010}{T}\right) - 1.3246}\right) * 1E^{-4} \qquad \text{(T, air temperature in K)} \qquad (16)$$

9. **2.3 An independent appraisal of photo-production rates**

10. Independently from NEMO-PISCES, the photochemical model of Fichot and Miller (2010)

11. was used to calculate monthly climatologies of depth-integrated photo-production rates of

12. OCS in the global ocean. Briefly, the photochemical model used three components to

13. calculate depth-resolved photochemical rates in the global ocean: 1) a radiative transfer model

14. for the determination of cloud-corrected UV-visible (290-490 nm) downward scalar

15. irradiance, 2) the SeaUV algorithm (Fichot et al., 2008), used to calculate the spectral diffuse

16. attenuation coefficient of UV and CDOM absorption coefficient (290-490 nm) from satellite

17. ocean color data, and 3) published AQY for the photochemical process of interest. To

18. describe the observed variability in AQY, both mean values from Weiss et al. (1995a) (open

19. ocean) and that of Zepp et al. (1994) (coastal ocean) were used in this study. Small

20. modifications to the original photochemical model were also made, including the use of

21. MODIS *Aqua* ocean color data (instead of SeaWiFS), and the use of a 2 nm spectral

22. resolution (instead of 5 nm). The photoproduction rates are later compared to the NEMO-

23. PISCES simulated rates and to other seawater measurements (e.g. Cutter et al., 2004).

24.

25. **3 Results**

26. The absorption coefficient of CDOM at 350 nm (a_{350}) increased monotonically with

27. chlorophyll concentration for low chlorophyll contents. The different a_{350}-chlorophyll

28. relations used in this paper led to large differences in a_{350} estimates, especially at high

29. chlorophyll levels in seawater (Fig. 3). Estimates of a_{350} obtained with the relation based on

30. MODIS aqua ocean color, that we proposed (Eq.(6)), provided values two to three times

larger than a_{350} values obtained with the relation from Preiswerk et al. (2000). Since both photo- and dark-production are modeled as linear functions of a_{350}, underestimating/overestimating chlorophyll concentrations directly lead to underestimated/overestimated OCS production. Therefore, the evaluation of chlorophyll concentration is of capital importance in the present work.

3.1 Evaluation of chlorophyll concentration at the global scale

Modeled annual mean surface chlorophyll concentrations from NEMO-PISCES compared relatively well with SeaWiFS chlorophyll observations (Fig.4). The model correctly represented main spatial patterns with for instance high latitudes showing higher annual mean chlorophyll concentrations and a stronger seasonal cycle. Observed mid- and high-latitude chlorophyll levels showed values three to four times larger than chlorophyll levels in tropical regions, which was also well captured with NEMO-PISCES. However, the model generally underestimated the chlorophyll concentration in the most oligotrophic subtropical zones of the global ocean.

3.2 Evaluation of the depth-distribution of a_{350} and OCS concentrations

In order to provide an evaluation of modeled vertical distributions of OCS concentrations, in this subsection we present vertical monthly mean profiles of a_{350} and OCS concentration from 1D simulation runs with NEMO-PISCES. Wherever possible, we compared these simulated profiles with relevant in situ measurements. A majority of them were taken in the site of BATS (31°N, 64°W). In situ measurements for OCS concentrations remain scarce at this point. Evaluations of the contribution of each individual OCS formation and destruction processes are even scarcer. Therefore, the cruise measurements around the BATS site from Cutter et al. (2004) are often used as a reference.

3.2.1 Vertical profiles for a_{350}

Our MODIS-*Aqua* based extrapolation (Eq. (6)) resulted in the highest values of simulated a_{350} (up to 0.15 m^{-1}, both in January and in August), while the parameterization from Preiswerk et al.(2000) resulted in a_{350} values that were about half as much (Fig. 5), consistent with the difference in the respective a_{350}-chlorophyll formulations (Fig. 3). Values for a_{350} deduced from Morel and Gentili (2009) (Eq. (2)) gave an intermediary result. The pronounced August maximum around 80 m depth (Fig. 5, B) reflected a chlorophyll content maximum at this depth (a_{350} is monotonically increasing for low levels of chlorophyll). In contrast, low a_{350}

values near the surface translated to a local minimum in the chlorophyll content. Note also the abrupt decrease of chlorophyll concentrations, and therefore the decreasing a_{350}, for depths below 80 m in August. In January the mixed layer was 120m-thick in NEMO-PISCES at the BATS site (Fig. 5, A). Chlorophyll content (thus a_{350}) remained high and constant over the first 120 m of the ocean before an abrupt decrease in the pycnocline. For both January and August, chlorophyll concentrations and a_{350} values became negligible below 200m, with the exception of a_{350} calculated with the relation proposed in this work.

3.2.2 Vertical OCS concentration profiles

Differences in a_{350} estimations using the relations in Eq. (2) to Eq. (6) led to 3-fold difference between the most extreme near-surface OCS maximum concentrations simulated by NEMO-PISCES (from 100 to 300 pmol L^{-1} in August and from 30 to 85 pmol L^{-1} in January). In the photic zone (the first 30 m below the surface, as implemented in NEMO-PISCES), August subsurface OCS concentrations (Fig. 5, D) were clearly driven by the photo-production (vertical profile of photo-production not shown here). Where the influence of UV-light irradiance is smaller or negligible (below 30 m in August or in the entire water column in January), OCS concentration profiles are driven by the predominant dark-production (vertical profile of the dark-production contribution not shown here). Therefore, in these layers, OCS concentrations mostly followed the chlorophyll content profiles. Thus, OCS concentration profiles simulated with NEMO-PISCES in January showed a drop below the mixed layer (below 120m), and became negligible below 200m. In August, the highest concentrations were found at the surface. A second peak of OCS levels was found around 80 m depth, where chlorophyll content peaks. Deeper, the OCS concentrations decreased, down to negligible values below 200m.

OCS concentrations simulated with NEMO-PISCES showed very large values in the few first meters under the surface, averaging 70, 90 or even 270 pmol L^{-1} in August at BATS site, depending on the a_{350}-chlorophyll relation used. Some OCS levels measured with buoys during a field campaign in August 1999 at BATS peaked at 150 pmol L^{-1} in the first 3 meters (Cutter et al. 2004), showing a potential to reach such high values. When using the a_{350} formulas derived from the studies of Morel and Gentili (2009) or Preiswerk (2000), the simulated vertical profiles of OCS concentrations in the Sargasso Sea in August (Fig. 5D) fall into the range of measured OCS concentrations reported by Cutter et al. (2004). This is

however not the case when using the a_{350} based on MODIS-aqua data which lead to the highest simulated OCS concentrations (270 pmol L^{-1} at the sea surface) and seem to overestimate the natural variability of the OCS concentrations, as measured in these waters.

The lower OCS concentrations in deeper layers reflected the quick removal of OCS by hydrolysis in the model (vertical profile of the hydrolysis contribution not shown here). This behavior fit well with the estimated short lifetime of the OCS molecule in marine waters, ranging between 4 and 13.4 hours, according to the models of Elliot et al. (1989) and Radford-Knoery and Cutter (1993), respectively.

3.3 Spatial and seasonal variability of OCS production and removal processes

3.3.1 Surface a_{350} patterns

Absorption coefficients of CDOM at 350 nm (a_{350}) simulated using NEMO-PISCES were evaluated for the different formulations of a_{350} against the annual climatology of *a_{350}* derived from MODIS *Aqua* ocean color as in Fichot and Miller (2010). The MODIS *Aqua*-derived *a_{350}* (Fig. 6, panel A) showed minimal values in the subtropical gyres, and maximum values in coastal regions and at high latitudes (higher than 45°N and 45°S). Note that the MODIS Aqua derived values should not be considered as direct observations but only as an independent estimate relying on a generic relation (i.e., a statistical model).

Regions where a_{350} was not accurately modeled also suffered from biases in simulated chlorophyll values. Therefore the highest a_{350} values observed near the coasts were not represented in NEMO-PISCES due to its limited spatial resolution. Additionally, the simulated chlorophyll maps (thus those of a_{350} as well) showed a higher contrast between low and high latitudes than the SeaWiFS derived observations (Fig. 4). In tropical regions (30°S-30°N), especially in the Atlantic Ocean, the Indian Ocean and in the Western Pacific Warm Pool, chlorophyll levels simulated by NEMO-PISCES were underestimated by a factor of two compared to the SeaWiFS chlorophyll observations (Fig. 4). As these are regions of warm ocean waters favorable to OCS dark-production, the consequence might be an underestimation of OCS production in these regions. In regions showing low chlorophyll concentrations, this underestimation translates to an approximately 30% underestimation of the a_{350} value (depending on the a_{350} formulation used), which directly translates to an equivalent underestimation of OCS dark- and photo-production, since both parameterization linearly depend on a_{350}.

Finally, NEMO-PISCES-simulated chlorophyll levels at mid- and high-latitudes were similar for northern and southern oceans, with average values around 0.5 mg m^{-3}. However, chlorophyll concentrations deduced from satellite observations showed average mid- and high-latitude values around 0.2 mg m^{-3} in the Southern Hemisphere and 0.5 to 1 mg m^{-3} in the Northern Hemisphere. Thus, the NEMO-PISCES model overestimated the chlorophyll concentrations by a factor of 2 over most of the mid- and high-latitudes of the Southern Hemisphere - especially in the Pacific Ocean and south of Australia (Fig. 4). Therefore, our modeled OCS production in the Southern Hemisphere is likely overestimated.

The different a$_{350}$-chlorophyll relations used in the present work (Eq. (2), Eq. (3) and Eq.(6)) led to simulated values of a$_{350}$ differing by as much as a factor of three. The CDOM absorption coefficient values obtained with the formulations of Preiswerk et al. (2000) and Morel and Gentili (2009) were similar to the MODIS-derived estimates for low- and mid-latitudes (below 60°S and 60°N), but largely underestimated at high latitudes in the Northern Hemisphere, with values two to three times smaller than the MODIS-derived estimates (Fig. 6). Conversely, the formulation presented in this work (Eq. (6)) correctly reproduced the observed levels of a$_{350}$ in the northern high latitudes, but clearly overestimated the values for CDOM absorption coefficient at low latitudes and in the Southern Hemisphere: simulated a$_{350}$ values in some subtropical oligotrophic regions reached values three to four times higher than the MODIS derived values.

3.3.2 Photo-production rates

In the present study, the a$_{350}$-dependent NEMO-PISCES model and the AQY dependent photochemical model from Fichot and Miller (2010) were used to provide two independent estimates of OCS photo-production rates. Sensitivity tests were performed on the annual global OCS photo-production over the entire water column (from the sea surface to the ocean floor). Both models were run with different formulations of a$_{350}$ (NEMO-PISCES model) or using different AQY (Fichot and Miller photochemical model) from the literature.

The AQY estimates used were collected in open ocean environments (Weiss et al., 1995a) and coastal environments (Zepp et al., 1994), respectively. Large uncertainties around AQY estimations depending on the measurement location led to large differences in the estimates of global OCS photo-production. Global OCS photo-production modeled with Fichot and Miller's model (2010) thus ranged from 876 to 5,500 GgS yr^{-1} (Table 1). Extremely high AQY values have been measured on the continental shelf (Cutter et al., 2004), but were not considered appropriate to represent the global average ocean. Using this last value would have

1   led to 37,700 GgS yr^{-1} of OCS global photoproduction, far above observed photo-production

2   levels and other model estimates.

3   Both the photochemical model from Fichot and Miller (2010) and the NEMO-PISCES model

4   led to similar spatial distributions of OCS photo-production (Fig. 7). Indeed, subtropical

5   regions are the major contributors in terms of yearly total photo-production of OCS, because

6   the photo-production rates were roughly constant through the entire year, whichever model

7   was used. However, the highest monthly photo-production rates were found in mid-latitude

8   regions (40-60°N and 40-60°S) during the period of maximum irradiance, with rates twice as

9   large as the nearly constant rates obtained in tropical regions, as can be seen in the time-

10 latitude diagram in Fig. 8 (panel A). Depending on the value of the driving parameter for the 2

11 models used (AQY or a_{350}, respectively), large uncertainties existed over the total quantities

12 of OCS photo-produced. Global photo-production of OCS for the NEMO-PISCES model and

13 the photochemical model from Fichot and Miller (2010) are compared in Table 1. When using

14 the a_{350}-based model NEMO-PISCES, the range of the global OCS photo-production was

15 reduced but still large, with estimates between 1,390 and 4,540 GgS yr^{-1}, depending on which

16 formulation was chosen to calculate a_{350}. These values were in rather good agreement with the

17 range obtained with the AQY-based photochemical model from Fichot and Miller (2010).

18 The photochemical model from Fichot and Miller and NEMO-PISCES showed lower OCS

19 photo-production rates than in situ measurements, irrespective of the a_{350} formulation. For

20 instance, Cutter et al. (2004) estimated August photo-production rates up to 10 or 15 pmol L^{-1}

21 h^{-1} in the Sargasso Sea, which is above the values of 4 to 9 pmol L^{-1} h^{-1} obtained by running

22 the NEMO-PISCES model at the same location (with implemented Eq. (3) and Eq. (6)

23 respectively) (Fig. 7).

24 **3.3.3 Dark-production rates**

25 Dark-production is a linear function of a_{350} (Eq. (8)). However, temperature is the main driver

26 of global OCS dark-production as simulated by NEMO-PISCES. The time-latitude

27 representation of dark-production rates (Fig. 8, panel B) showed that the maximum values

28 were located at low latitudes, in warm marine waters, despite the fact that these regions

29 correspond to the lowest a_{350} values (Fig. 6). The dark-production rates in these regions

30 remained relatively constant throughout the year. On the contrary, chlorophyll-rich waters at

31 higher latitudes, leading to higher a_{350} values (Fig. 6) corresponded to colder marine waters

32 and thus limited dark-production rates (due to the temperature dependency in Eq. (8)).

Measurements from Von Hobe et al. (2001) at the BATS site showed dark-production rates of 1 to 1.5 pmol $L^{-1} h^{-1}$. NEMO-PISCES results showed a very good agreement with this data, with rates of 0.8 pmol $L^{-1} h^{-1}$ in August at BATS (not shown). In the study of Cutter et al. (2004), calculated dark-production rates reached 4 pmol $L^{-1} h^{-1}$ in August, significantly above the simulated range by NEMO-PISCES. Von Hobe et al. (2001) estimated that dark-production produces around 50% of OCS at these low latitudes. In the NEMO-PISCES model, dark-production only represented 34% of the OCS produced at low latitudes, and 66% of OCS is photo-produced.

3.3.4 Hydrolysis rates

Figure 2 presents the hydrolysis reaction constant as a function of temperature for a given pH, as given by the Kamyshny et al. (2003) and Elliott et al. (1989) formulations. Both formulations relate the OCS hydrolysis to the OCS concentration and to the seawater pH (Eq. (10a) and Eq. (10b)). At a given pH, the difference between the two formulations was leading to a 50% difference in the hydrolysis constant for seawater temperatures above 12°C (Fig. 2). A comparison between time-latitude maps of the hydrolysis rate (Fig. 8, panel C) and the OCS concentration (in Fig A1) suggests that OCS hydrolysis rates in NEMO-PISCES are largely driven by OCS concentrations. These spatio-temporal variation patterns only slightly differ around the equator, where marine waters are somewhat less alkaline, which leads to a limitation of the OCS hydrolysis rate through pH influence. Simulations run with two different hydrolysis parameterizations (based on Eq. (10a) or Eq. (10b)) provide global OCS emissions diverging by a factor of 2.5 (see Fig. 9).

3.3.5 Evaluation of surface concentration patterns

Maps of annual mean surface OCS concentration patterns at sea surface simulated with NEMO-PISCES are presented on Fig. 10 (right column). NEMO-PISCES simulations produced maximum annual mean OCS levels in equatorial and sub-tropical regions, where dark-production was maximal and photo-production was constantly active. In low latitude marine waters, OCS concentrations remained nearly constant throughout the year (Fig A1 and Fig. 10). However, the model showed a strong seasonal variability of OCS concentrations for mid- and high latitudes, with roughly a factor 10 difference between maximal and minimal OCS concentration levels reached throughout the year. These spatial distributions and the intra-annual variation amplitudes were relatively independent of the formulation used in NEMO-PISCES to calculate a_{350}.

Modeled OCS concentrations were evaluated against observational data available in the literature. OCS concentrations measured near European shores and estuarine regions over the year, showed large spatial and temporal variability (Uher, 2006). The few measured OCS concentrations in estuarine regions were close to 250 pmol L^{-1} in winter and 430 pmol L^{-1} in summer, while smaller values were measured near shores, from 40 pmol L^{-1} in winter to 100 pmol L^{-1} in summer. Von Hobe et al. (2003) also measured summer OCS surface maximum levels of 120 pmol L^{-1}, in an upwelling region near the Portuguese coast. When using the MODIS-*Aqua*-based a$_{350}$ formulation (Eq. (6)) which gives the best representation of a$_{350}$ in the region (Fig.6), simulated OCS concentrations near shores only reached values from 30 pmol L^{-1} in winter to 100 pmol L^{-1} in summer (Fig. 10). NEMO-PISCES matches correctly the seasonal amplitude of OCS concentrations measured in these areas and represents quite accurately the absolute values measured near the shores. However, as expected, the lack of resolution of the model translates into an under-estimation of the estuarine concentrations.

As shown in the comparison done in the study of von Hobe et al. (2003), the reproduction of the OCS depth profiles by their models was generally less accurate than that of surface data because the models were tuned to fit the surface concentrations. In our study, the model was not tuned to fit surface or depth concentrations. As NEMO-PISCES provides gridded monthly mean concentrations of OCS on the entire water column, monthly mean concentrations of OCS data series should, ideally, be used to evaluate the global simulations.

Unfortunately, a global database of sea surface OCS measurements and a procedure to calculate sea surface OCS as a function of latitude, longitude, and month are not available in the literature as, for example, for DMS (e.g. Kettle et al., 1999; Lana et al, 2011). The assemblage of a global OCS database was not achievable in the framework of this project. The evaluation of the modeled oceanic OCS concentrations that had been carried out is not fully satisfactory because we implicitly accepted to compare modeled monthly mean concentrations and discrete measurements.

With these caveats in mind, 150 OCS measurements classified according to location, date and depth were gathered from the literature (Weiss et al., 1995a ; Ulshofer et al., 1996 ; Cutter et al., 2004 ; Von Hobe et al., 2001 and 2003) and compared with the outputs from the model run with its "standard" parameterization, as described in the discussion section. The results are displayed in Fig. A2 and show that the outputs of the model generally overestimate the measured concentrations by a factor of two to four at the sea surface (first 10m, A), especially at sites where low concentrations were measured. In seawaters with high OCS concentration

measurements (higher than 100 pmol L^{-1}), the corresponding simulated concentrations were generally underestimated, up to a factor of two. A better agreement between modeled and observed concentrations is found with the subsurface data (below 10m, B).

This model-data comparison suggests that simulated OCS concentrations might be overestimated in a significant way in surface waters, which might lead to an overestimation of the simulated OCS outgassing fluxes (up to factors of two to four). However, the limited spatial (many measurements were done around 40°N) and temporal (many measurements in July and August) distribution of the measurements severely reduced the possibility for an exhaustive model validation and for the identification of concentration biases in the model. Furthermore, a large range of concentrations were measured even for sites close in latitude and/or for measurements realized around the same period of the year. Finally, this over-estimation might also compensate for the under-estimation in the OCS production in shallow water, since the model is lacking an exhaustive representation of the estuarines regions.

The formulation used to calculate a_{350} values did not affect the global spatial distribution of OCS concentrations, but it largely influenced the absolute value of the simulated OCS concentrations. For instance, maximal OCS concentrations in tropical sub-surface waters were estimated close to 300 pmol L^{-1} with the MODIS-*Aqua*-based a_{350} formulation (Eq. (6)), while Morel and Gentili (2009) (Preiswerk et al., 2000)-based estimates only reached one half (one third, respectively) of these modeled maximal concentrations (Fig. 10). Note that the formulation of Morel and Gentili (2009) led to results that were in better agreement with the campaign measurements described in section 3.2.2 (Cutter et al, 2004; von Hobe et al., 2001).

4 Discussion

The limited number of studies which have attempted to quantify OCS production and removal processes individually have yielded widely differing results. Several parameterizations for each process have been proposed and each parameterization remains poorly constrained. In this section we present our "best guess" formulations for the individual OCS-related processes in the NEMO-PISCES model.

Measurement campaigns used to determine dark-production functions are particularly scarce. The dark-production parameterization that we used is related to the CDOM absorption coefficient at 350 nm, as a parameterization of the link with organic matter content and biological activity in marine environments. However, there is no rationale for dark-production

1   to be dependent of colored organic matter content (CDOM, chlorophyll) since this process

2   occurs at times when no light is available.

3   In a rare example of observation-based dark-production parameterization effort, von Hobe et

4   al. (2003) used an experimental setup that allows them to equate the OCS dark-production

5   rate to the hydrolysis rate, and thus expressed the first as a function of a measurement of the

6   latter. In their estimate of the hydrolysis rate, von Hobe et al. (2003) use the Elliott et al.

7   (1989) formulation for the OCS hydrolysis constant. Thus, our use of the von Hobe et al.

8   (2003) dark-production parameterization is consistent with the choice of the Elliott et al.

9   (1989) parameterization for OCS hydrolysis.

10   As previously described, simulated a_{350} values can be far from the observed values in warm

11   water regions depending on the a_{350} formulation used (Fig. 6). This potentially leads to the

12   largest errors in the dark-production rate estimates. In this context, we have found the Morel

13   and Gentili (2009) a_{350} parameterization to perform best when evaluated against a_{350} values

14   derived from MODIS-*Aqua* data at low latitudes, as well as at high latitudes in the Southern

15   Hemisphere (section 3.3.1). This formulation may, however, lead to an underestimation of

16   a_{350} at high latitudes in Northern Hemisphere.

17   We have chosen the Uher et al. (1997) formulation for photoproduction associated with the

18   Morel and Gentili parameterization for a_{350} (Eq. (2)) and the Elliott formulation for the

19   hydrolysis constant as the standard parameterizations for OCS processes in NEMO-PISCES,

20   based on the arguments above. Time-latitude diagrams for photo- and dark-production,

21   hydrolysis and surface OCS fluxes using these parameterizations are represented in Fig. 8.

22   The time-latitude diagram representing the surface layer OCS concentration with the same

23   settings is shown in Fig A1.

24   The standard run of NEMO-PISCES suggests most OCS is produced photochemically. Even

25   at low latitudes, where warm water regions favor dark-production of OCS, photo-production

26   represents 66% of OCS production pathway (Fig. 8). In this simulation, low latitudes are the

27   only regions where dark-production rates compensate for hydrolysis removal of OCS. The

28   highest annual mean OCS concentrations modeled using best guess parameterizations range

29   between 100 and 200 pmol L^{-1} and are encountered around the equator, especially in Central

30   and Eastern Pacific Ocean. At mid and high latitudes, simulated annual mean OCS

31   concentrations are included between 10 and 60 pmol L^{-1}. These regions show higher seasonal

32   amplitude in OCS concentrations, especially around 60°N and 40°S, where periods of

irradiance maxima (resp. minima) lead to simulated OCS concentrations of 150 pmol L^{-1} (resp. 10 pmol L^{-1}). In these regions, simulated concentrations are largely consistent with in situ measurements from Cutter et al. (2004) and Von Hobe et al. (2003).

Surface OCS concentrations simulated by NEMO-PISCES are the main driver of the model's sea-air OCS fluxes (Fig. 8, panel D and Fig A1). The regions with the highest sea surface OCS concentrations (tropics and mid-latitudes during maximal irradiance seasons) are the regions emitting the largest quantities of OCS. Multiple measurement campaigns (Rasmussen, Khalil and Hoyt, 1982; Ferek and Andreae, 1983; Uher, 2006) have shown that coastal environments can have OCS concentrations 5 to 10 times higher than those measured at the surface of open ocean waters in oligotrophic regions. As shown in Fig.6, MODIS-derived a$_{350}$ reach maximal values along shores but the NEMO-PISCES model does not represent these localized maxima due to the poor model resolution in these regions. These narrow areas have an important potential in OCS production and show under-estimated OCS concentrations in NEMO-PISCES.

Air-sea exchange of OCS is also enhanced by warm surface waters and strong winds (Eq. (11)). Both variables have a noticeable impact on the simulated OCS surface fluxes, especially at low latitudes. In fact, NEMO-PISCES simulations show the highest OCS emissions around the equator even if some mid- and high-latitude oceanic regions show higher OCS sea surface concentrations for some periods of the year: OCS outgassing rates in July along the Equator are twice as important as outgassing taking place in Northern mid-latitudes in the same period (Fig. 8, panel D), despite the mid-latitudes showing surface OCS concentrations 60% higher than those simulated around the Equator.

We have investigated the sensitivity of the sea-air fluxes to the parameterizations of OCS production and removal processes. Global and regional annual sea-air OCS fluxes obtained in these tests are summarized in Fig. 9. Simulated fluxes by Kettle et al. (2002) are also represented on the figure 9 (black line) for comparison. While the different parameterization choices lead to a large spread in the simulated OCS fluxes towards the atmosphere, NEMO-PISCES consistently produces higher estimates of the global sea-air OCS fluxes than the ones previously estimated by Kettle et al. (2002). Total emitted OCS simulated using the "best guess" parameterization of NEMO-PISCES reaches 813 GgS yr^{-1}, far above the modeled direct source of 40 GgS yr^{-1} from Kettle et al. (2002) and consistent with the revised global oceanic flux based on atmospheric measurements and a model for leaf uptake, proposed by

Berry et al. (736 GgS yr^{-1}). Extrapolations of measurements carried out in the Mediterranean sea and the Indian ocean by Mihalopoulos et al. (1992) led to an independent estimate of 213 GgS yr^{-1}, markedly lower than the mean annual global flux simulated with NEMO-PISCES. Kettle et al. (2002) described the global direct exchange of OCS between the ocean and the atmosphere as highly uncertain, and pointed out the fact that in some of their simulations, some regions of the ocean behaved like sinks of atmospheric OCS at certain periods of the year. Some regions at extreme high latitudes also act like a sink of atmospheric OCS in NEMO-PISCES for certain periods of the year (Fig. 8, panel D).

9 - The different parameterizations available for the different processes presented in this paper lead to different global flux estimates, ranging from 573 GgS yr^{-1} (when using the CDOM absorption coefficient values obtained with the formulations of Preiswerk et al. (2000) and the higher values of the Elliot-based hydrolysis constant) to 3997 GgS yr^{-1} (when using the MODIS-derived a_{350} and the lower values of the Kamyshny-based hydrolysis constant). Our "best-guess" parameterization of NEMO-PISCES shows the best agreement with the in situ evaluation of the individual processes, and stands in the lower part of the range of OCS direct annual emissions by ocean at a global scale.

17 - Changing the parameterization also changes the seasonal amplitude of the simulated OCS flux by up to a factor five for Northern and Southern Hemisphere oceans but no significant change is noticeable on the seasonal amplitude of OCS fluxes in the tropical region.

Recent efforts to constrain global OCS fluxes have led to a growing number of measurements and consequent revisions of soil and vegetation uptake estimates. Multiple recent studies have suggested that soil and vegetation uptakes were underestimated in the new assessments of the global OCS cycle and have suggested a global sink for both of up to 1000 GgS yr^{-1} (Berry et al., 2013; Suntharalingam et al., 2008), much larger than the estimates of approximately 300 GgS yr^{-1} by Kettle et al. (2002). Knowing that atmospheric OCS levels show no trend over the last two decades (Montzka et al., 2007), the global cycle of OCS is expected to be balanced on a global scale. In order to compensate re-estimated sinks based on a mechanistic description of leaf OCS uptake (using SIB3 land surface model), Berry et al. (2013) have suggested that the ocean provides the missing source. Using a simple inversion approach to optimize the oceanic missing source, given known land natural and anthropogenic fluxes, the authors evaluated that the ocean should emit 736 GgS yr^{-1}. Moreover, the best-fit optimization used by the authors revealed that the missing source should be concentrated over the low latitudes in order to best fit the atmospheric data recorded at NOAA stations.

Using our "best guess" parameterization for NEMO-PISCES leads to relatively constant global OCS outgassing throughout the year, with a seasonal amplitude of only 10%. Tropical regions (30°S-30°N) emit the major part of the OCS, and represent up to 45% of the total emitted OCS towards the atmosphere. Tropical exchanges show almost no variation throughout the year. Northern and southern oceanic regions at mid- and high latitudes (higher than 30°N and 30°S, respectively) contribute to 20% and 35%, respectively, of the OCS global flux towards atmosphere each year (Fig A3).

Despite the consistency in terms of global OCS fluxes quantities and spatial distribution between best guess parameterizations of NEMO-PISCES and indirect oceanic source estimate from Berry et al. (2013), the simulated outgassing using NEMO-PISCES show a large envelope when using the different possible parameterizations. Most of them lead to much larger global flux estimates than previous studies, ranging between 573 and 3997 GgS yr^{-1}. Higher estimates for OCS fluxes with NEMO-PISCES result from using hydrolysis constant from Kamyshny et al. (2003) or a_{350} calculation proposed in this present work. Kamyshny-based hydrolysis constant is not homogeneous with the choice of an Elliot-based hydrolysis constant used to determinate OCS dark-production by von Hobe et al. (2001), as implemented in NEMO-PISCES. Moreover, calculation of a_{350} proposed in this work was demonstrated to lead to large over-estimations of the a_{350} values compared with the observational data. Both parameterizations lead to very large estimates of OCS fluxes towards the atmosphere, which are not likely since they would lead to highly unbalanced atmospheric OCS budget.

5 Conclusion

At a global scale, the ocean is supposed to be the largest direct and indirect source of OCS to the atmosphere. Recent studies (Suntharalingam et al., 2008; Berry et al., 2013) pointed out the need to re-evaluate the global OCS sinks, signaling a possible underestimation in previous assessments. There is currently no trend in the atmospheric levels of OCS (Montzka et al., 2007), thus increased sinks have to be compensated by a source, currently missing from the global OCS budget. The recent inversion study of Berry et al. (2013) and previous Atmospheric Chemistry Experiment ACE observational analysis of Barkley et al. (2008) have suggested that a large part of this missing source should be ocean outgassing at low latitudes. Previous studies of the OCS production and removal processes in the ocean have only led to poor constraint of the potential global sea-air fluxes. Moreover, numerical simulations have

led to relatively small modeled global fluxes of OCS outgassed to the atmosphere. In this study we have selected different parameterizations for the most important OCS production and removal processes, which we then implemented in the 3D NEMO-PISCES ocean model. Simulated fluxes with this model showed a potential for large global OCS fluxes, with our best guess simulation reaching a net emission of OCS up to 800 GgS yr^{-1}, much larger than previous estimated ranges. Moreover, the resulting spatial distribution of theses fluxes supports the assumed key role of tropical regions, where warm marine waters can produce high levels of OCS with little organic matter. Our modeled ocean-atmosphere OCS fluxes were concentrated in the equatorial and subtropical regions, which accounted for half of the global OCS outgassing to the atmosphere. This result is in good agreement with the necessary distribution of the missing oceanic source of OCS that would be consistent with the atmospheric OCS concentration gradients (north south gradient for instance), measured at the different stations of the NOAA network. The uncertainties around OCS fluxes, however, will remain very large until a wide array of measurements focusing on the individual processes is available, to accurately calibrate the relative importance of each marine OCS production and removal process.

Authors contribution

S. Belviso and P. Peylin designed the experiments. T. Launois did the bibliography research for process parameterizations and developed the NEMO-PISCES specific OCS module code and performed the simulations with the help from L. Bopp. C. Fichot run tests with the SeaUV model that he developed, allowing comparison of OCS photo-production rates with the results obtained with NEMO-PISCES. T. Launois prepared the manuscript with contributions from all co-authors.

References

Aumont, O., and L. Bopp, Globalizing results from ocean in situ iron fertilization studies, GLOBAL BIOGEOCHEM CY, 20, GB2017, doi:10.1029/2005GB002591, 2006

Barnes, I., Becker, K. H., Patroescu, I. The tropospheric oxidation of dimethyl sulfide: A new source of carbonyl sulfide. GEOPHYS RES LETT., 21(22), 2389-2392, 1997

Bopp L., Aumont O., Belviso S., Blain S, Modelling the effect of iron fertilization on dimethylsulphide emissions in the Southern Ocean. DEEP-SEA RES PT II, 55(5), 901-912, 2008

Barkley M. P., Palmer P. I., Boone C. D., Bernath P. F. and Suntharalingam P., Global distributions of carbonyl sulfide in the upper troposphere and stratosphere. GEOPHYS RES LETT, 35, L14810, doi:10.1029/2008GL034270, 2008

Berry J., Wolf A., Campbell J. E., Baker I., Blake N., Blake D., Zhu, Z., A coupled model of the global cycles of carbonyl sulfide and CO2: A possible new window on the carbon cycle. J GEOPHYS RES-BIOGEO, 118(2), 842-852, 2013

Bricaud A., Babin M., Morel A., Claustre H., Variability in the chlorophyll-specific absorption coefficients of natural phytoplankton: Analysis and parameterization. J GEOPHYS RES-OCEANS, (1978–2012),100(C7), 13321-13332, 1995

Brühl C., Lelieveld J., Crutzen P. J., Tost H., The role of carbonyl sulphide as a source of stratospheric sulphate aerosol and its impact on climate. ATMOS CHEM PHYS, 12(3), 1239-1253, 2012

Campbell J. E., Carmichael G. R., Chai T., Mena-Carrasco M., Tang Y., Blake D. R., Stanier C. O., Photosynthetic control of atmospheric carbonyl sulfide during the growing season. SCIENCE, 322(5904), 1085-1088, 2008

Chin M., Davis D. D., A reanalysis of carbonyl sulfide as a source of stratospheric background sulfur aerosol. J GEOPHYS RES-OC ATMOS (1984–2012), 100(D5), 8993-9005, 1993

Cutter G. A., Cutter L. S., Filippino K. C., Sources and cycling of carbonyl sulfide in the Sargasso Sea. LIMNOL OCEANOGR, 49(2), 555-565, 2004

Elliott S., Lu E., Rowland F. S., Rates and mechanisms for the hydrolysis of carbonyl sulfide in natural waters. ENVIRON SCI TECHNOL, 23(4), 458-461, 1989

Farmer, CT., Moore, C.A., Zika, R.G. and Sikorski, R.J., Effects of low and high Orinoco river flow on the underwater light field of the Eastern Caribbean Basin, J GEOPHYS RES (2279-2288), 98, 1993

Ferek R. J., Andreae M. O., Photochemical production of carbonyl sulphide in marine surface waters, GLOBAL BIOGEOCHEM CY, 6(2), 175–183, 1984

Fichot C. G., Miller W. L., An approach to quantify depth-resolved marine photochemical fluxes using remote sensing: Application to carbon monoxide (CO) photoproduction. REMOTE SENS ENVIRON, 114(7), 1363-1377, 2010

Fichot C. G., Sathyendranath S., Miller W. L., SeaUV and SeaUVC: Algorithms for the retrieval of UV/Visible diffuse attenuation coefficients from ocean color. REMOTE SENS ENVIRON, 112(4), 1584-1602, 2008

Flöck O. R., Andreae M. O., Dräger M., Environmentally relevant precursors of carbonyl sulfide in aquatic systems. MAR CHEM, 59(1), 71-85, 1997

Johnson J. E., Harrison H., Carbonyl sulfide concentrations in the surface waters and above the Pacific Ocean. J GEOPHYS RES-OC ATMOS (1984–2012), 91(D7), 7883-7888, 1986

Kamyshny A., Goifman A., Rizkov D., Lev O., Formation of carbonyl sulfide by the reaction of carbon monoxide and inorganic polysulfides. ENVIRON SCI TECHNOL, 37(9), 1865-1872, 2003

Kettle, A. J., et al. (1999), A global database of sea surface dimethylsulfide (DMS) measurements and a procedure to predict sea surface DMS as a function of latitude, longitude, and month, Global Biogeochem. Cycles, 13(2), 399–444, doi:

Kettle A. J., Kuhn U., Hobe M. V., Kesselmeier J., Liss P. S., Andreae M. O., Comparing forward and inverse models to estimate the seasonal variation of hemisphere-integrated fluxes of carbonyl sulfide. ATMOS CHEM PHYS, 2(5), 343-361, 2002

Kloster S., Feichter J., Maier-Reimer E., Six K. D., Stier P., Wetzel P., DMS cycle in the marine ocean-atmosphere system? a global model study. BIOGEOSCIENCES, 3(1), 29-51, 2006

Lana, A., et al. (2011), An updated climatology of surface dimethlysulfide concentrations and emission fluxes in the global ocean, Global Biogeochem. Cycles, 25, GB1004, doi:10.1029/2010GB003850

Large W. G., Yeager S. G., The global climatology of an interannually varying air–sea flux data set, CLIM DYNAM, 33, 341–364, 2008

Madec G., NEMO ocean general circulation model reference manuel. Internal Report. LODYC/IPSL, Paris, 2008

Mihalopoulos N., Nguyen B. C., Putaud J. P., Belviso S., The oceanic source of carbonyl sulfide (COS). ATMOS ENVIRON A-GEN, 26(8), 1383-1394, 1992

Morel A., Optical modeling of the upper ocean in relation to its biogenous matter content (case I waters). J GEOPHYS RES-OCEANS (1978–2012), 93(C9), 10749-10768, 1988

Morel A., Gentili B., A simple band ratio technique to quantify the colored dissolved and detrital organic material from ocean color remotely sensed data. REMOTE SENS ENVIRON, 113(5), 998-1011, 2009

Montzka S. A., Calvert P., Hall B. D., Elkins J. W., Conway T. J., Tans P. P., Sweeney, C., On the global distribution, seasonality, and budget of atmospheric carbonyl sulfide (COS) and some similarities to CO2. J GEOPHYS RES-OC ATMOS (1984–2012), 112(D9), 2007

Notholt J., Weisenstein D., Kuang Z., Rinsland C. P., Toon G. C., Rex M., Schrems O., Composition of the upper tropical troposphere and its influence on the stratospheric aerosol formation. EGS-AGU-EUG Joint Assembly (Vol. 1, p. 4024), 2003

1 Para J., Coble P.G., Charrière B., Tedetti M., Fontana C., Sempéré R., Fluorescence and
2 absoprtion properties of chromophoric dissolved organic matter (CDOM) in coastal surface
3 waters of the northwestern Mediterranean Sea, influence of the Rhône River.
4 BIOGEOSCIENCES, 7, 4083-4103, 2010

5 Preiswerk D., Najjar R. G., A global, open-ocean model of carbonyl sulfide and its air-sea
6 flux. GLOBAL BIOGEOCHEM CY, 14(2), 585-598, 2000

7 Radford-Knoery J., Cutter G. A., Determination of carbonyl sulfide and hydrogen sulfide
8 species in natural waters using specialized collection procedures and gas chromatography
9 with flame photometric detection. ANAL CHEM, 65(8), 976-982, 1993

10 Rasmussen R. A., Khalil M. A. K., Hoyt S. D., The oceanic source of carbonyl sulfide
11 (OCS). ATMOS ENVIRON (1967), 16(6), 1591-1594, 1982

12 Suntharalingam P., Kettle A. J., Montzka S. M., Jacob D. J., Global 3-D model analysis of the
13 seasonal cycle of atmospheric carbonyl sulfide: Implications for terrestrial vegetation
14 uptake. GEOPHYS RES LETT, 35(19), 2008

15 Tedetti M., Sempéré R., Penetration of ultraviolet radiation in the marine environment. A
16 review. PHOTOCHEM PHOTOBIOL, 82(2), 389-397, 2006

17 Uher G., Distribution and air–sea exchange of reduced sulphur gases in European coastal
18 waters. ESTUAR COAST SHELF S, 70(3), 338-360, 2006

19 Uher G., Andreae M. O., Photochemical production of carbonyl sulfide in North Sea water: A
20 process study. LIMNOL OCEANOGR, 42(3), 432-442, 1997

21 Ulshöfer V. S., Uher G., Andreae M. O., Evidence for a winter sink of atmospheric carbonyl
22 sulfide in the northeast Atlantic Ocean. GEOPHYS RES LETT, 22(19), 2601-2604, 1995

23 Ulshöfer V. S., Flock O. R., Uher G., Andreae M. O., Photochemical production and air-sea
24 exchange of carbonyl sulfide in the eastern Mediterranean Sea. MAR CHEM, 53(1), 25-39,
25 1996

26 Von Hobe M., Cutter G. A., Kettle A. J., Andreae M. O., Dark production: A significant
27 source of oceanic COS. J GEOPHYS RES-OCEANS (1978–2012), 106(C12), 31217-31226,
28 2001

29 Von Hobe M., Najjar R. G., Kettle A. J., Andreae M. O., Photochemical and physical
30 modeling of carbonyl sulfide in the ocean. J GEOPHYS RES-OCEANS (1978–
31 2012), 108(C7), 2003

32 Wanninkhof R., Relationship between wind speed and gas exchange over the ocean. J
33 GEOPHYS RES-OCEANS (1978–2012), 97(C5), 7373-7382, 1992

34 Watts S. F., The mass budgets of carbonyl sulfide, dimethyl sulfide, carbon disulfide and
35 hydrogen sulfide. ATMOS ENVIRON, 34(5), 761-779, 2000

36 Weiss P. S., Johnson J. E., Gammon R. H., Bates T. S., Reevaluation of the open ocean source
37 of carbonyl sulfide to the atmosphere. J GEOPHYS RES-OC ATMOS (1984–
38 2012), 100(D11), 23083-23092, 1995a

Weiss P. S., Andrews S. S., Johnson J. E., Zafiriou O. C., Photoproduction of carbonyl sulfide in South Pacific Ocean waters as a function of irradiation wavelength. GEOPHYS RES LETT, 22(3), 215-218, 1995b

Wohlfahrt G., Brilli F., Hörtnagl L., Xu X., Bingemer H., Hansel A., Loreto F., Carbonyl sulfide (COS) as a tracer for canopy photosynthesis, transpiration and stomatal conductance: potential and limitations†. PLANT CELL ENVIRON, 35(4), 657-667, 2012

Xu X., Bingemer H. G., Georgii H. W., Schmidt U., Bartell, U., Measurements of carbonyl sulfide (COS) in surface seawater and marine air, and estimates of the air-sea flux from observations during two Atlantic cruises. J GEOPHYS RES-OC ATMOS (1984–2012), 106(D4), 3491-3502, 2001

Zepp R. G., Andreae M. O., Factors affecting the photochemical production of carbonyl sulfide in seawater. GEOPHYS RES LETT, 21(25), 2813-2816, 1994
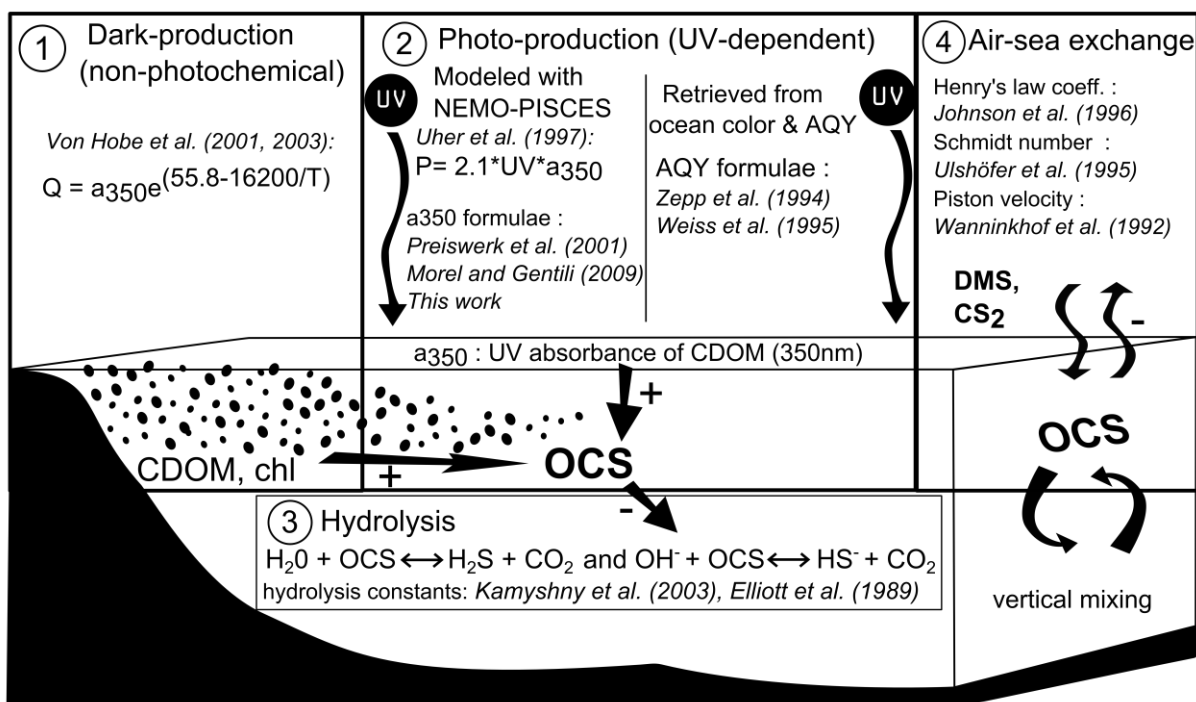
Figure 1: Main production and removal processes implemented in the NEMO-PISCES OGCM to simulate the marine OCS cycle: dark-production, photo-production and hydrolysis. Of central importance is the UV absorption coefficient at 350 nm of chromophoric dissolved organic matter (CDOM) which is derived from modeled Chl concentrations using three different relationships linking a_{350} to Chl. The simulated photo-production rates of OCS were evaluated independently using the model of Fichot and Miller (2010) and published apparent quantum yields (AQY). Aqueous OCS is removed by hydrolysis (two different formulations of the hydrolysis rate are used), lost or absorbed at the air-sea interface and mixed both vertically and horizontally. Studies relevant for sensitivity tests and model parameterization presented in this paper are displayed in italic. Oceans also emit DMS and CS_2 which are later oxidized in OCS in the atmosphere. These indirect sources of OCS are not detailed in the present study.
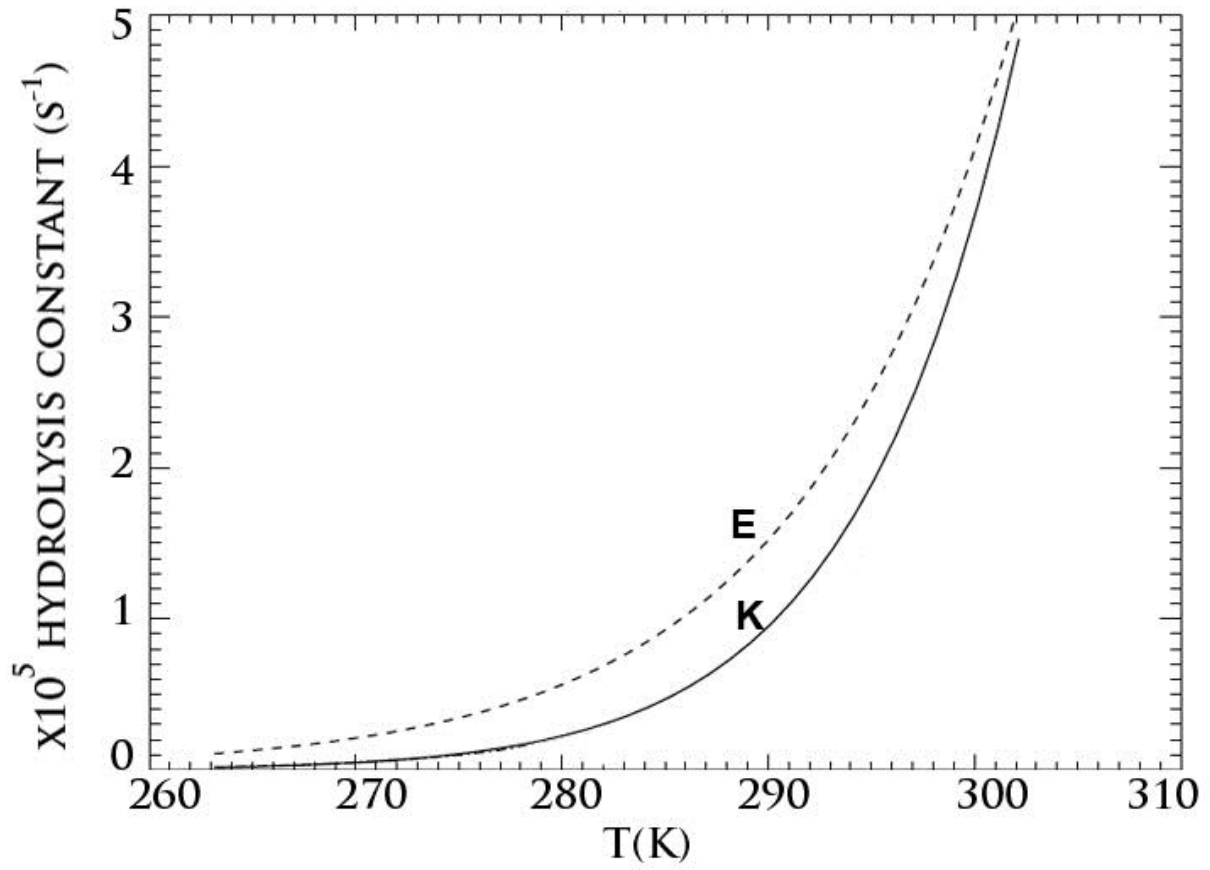
1

Figure 2: Temperature dependence of hydrolysis rates implemented in NEMO-PISCES. The
relationships are represented for pH = 8.2, and taken from Elliott et al. (1989) (E, dashed line)
or Kamyshny et al. (2003) (K, solid line). .

5

6

7

8

9

10

11

1
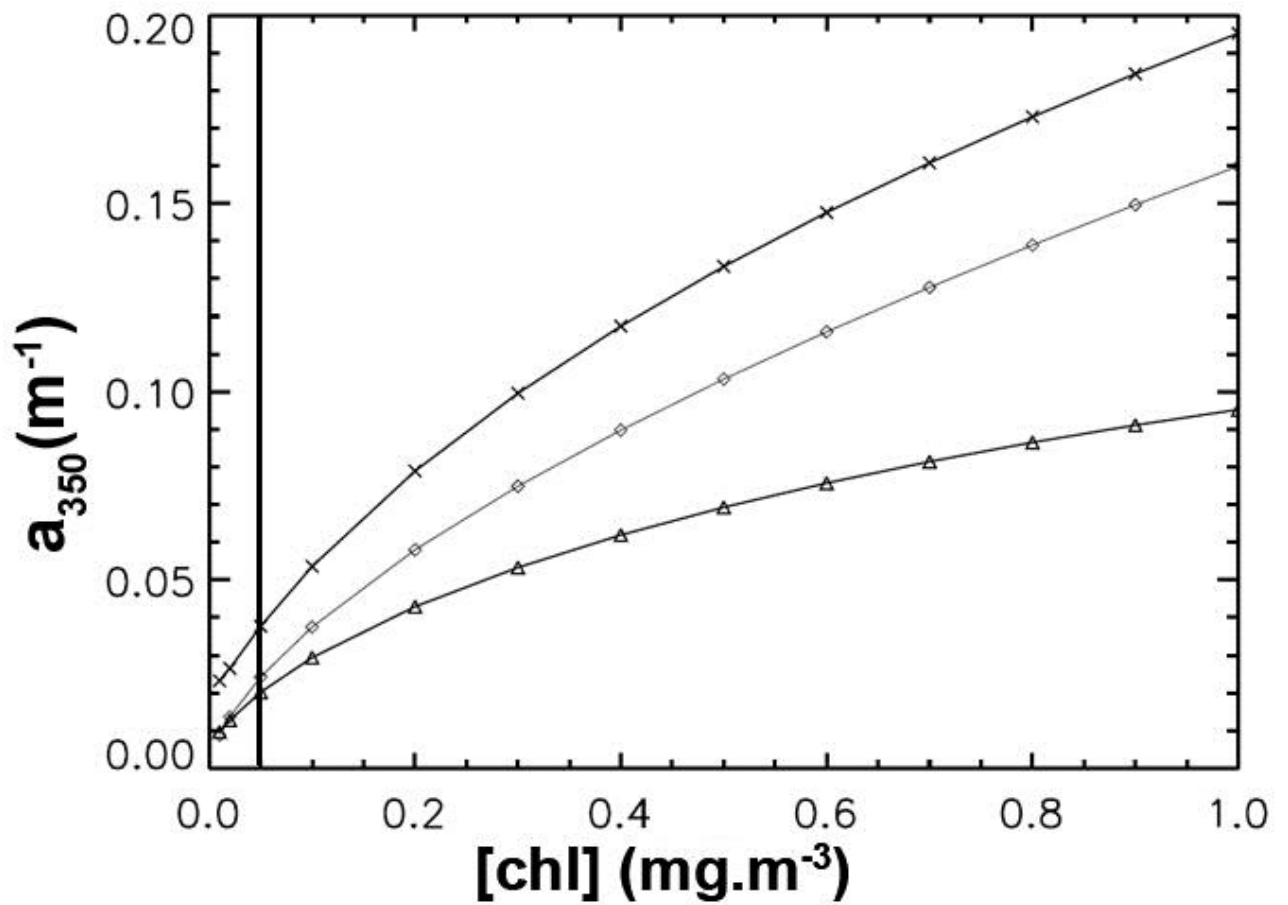
Figure 3: Relationships implemented in the NEMO-PISCES model between UV absorption
coefficients for CDOM at 350 nm and chlorophyll concentrations. The 3 respective
relationships are from Morel and Gentili (2009) (diamonds), Preiswerk et al. (2000)
(triangles) or issued from this study, based on MODIS-*Aqua* ocean color (crosses).
Chlorophyll concentrations in NEMO-PISCES have a fixed minimal value of 0.05 mg.m^{-3}
(thick vertical line).
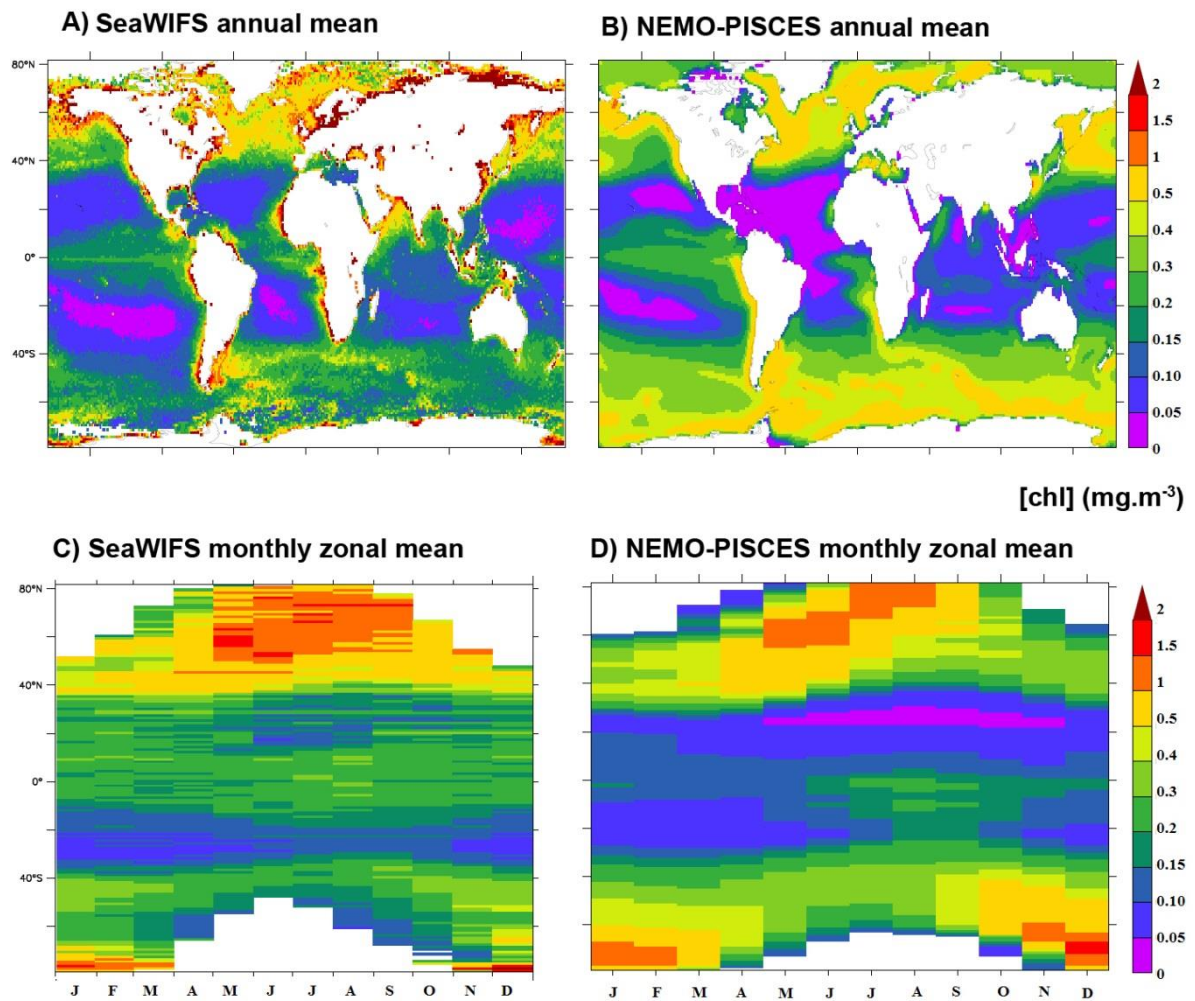
Figure 4: Comparison of remotely sensed observations of chlorophyll (left panels) with simulations performed using the NEMO-PISCES model (right panels). Top panels (a, b) represent maps of annual mean chlorophyll concentration (mg.m^{-3}). Bottom panels (c, d) represent latitude-time maps of chlorophyll.
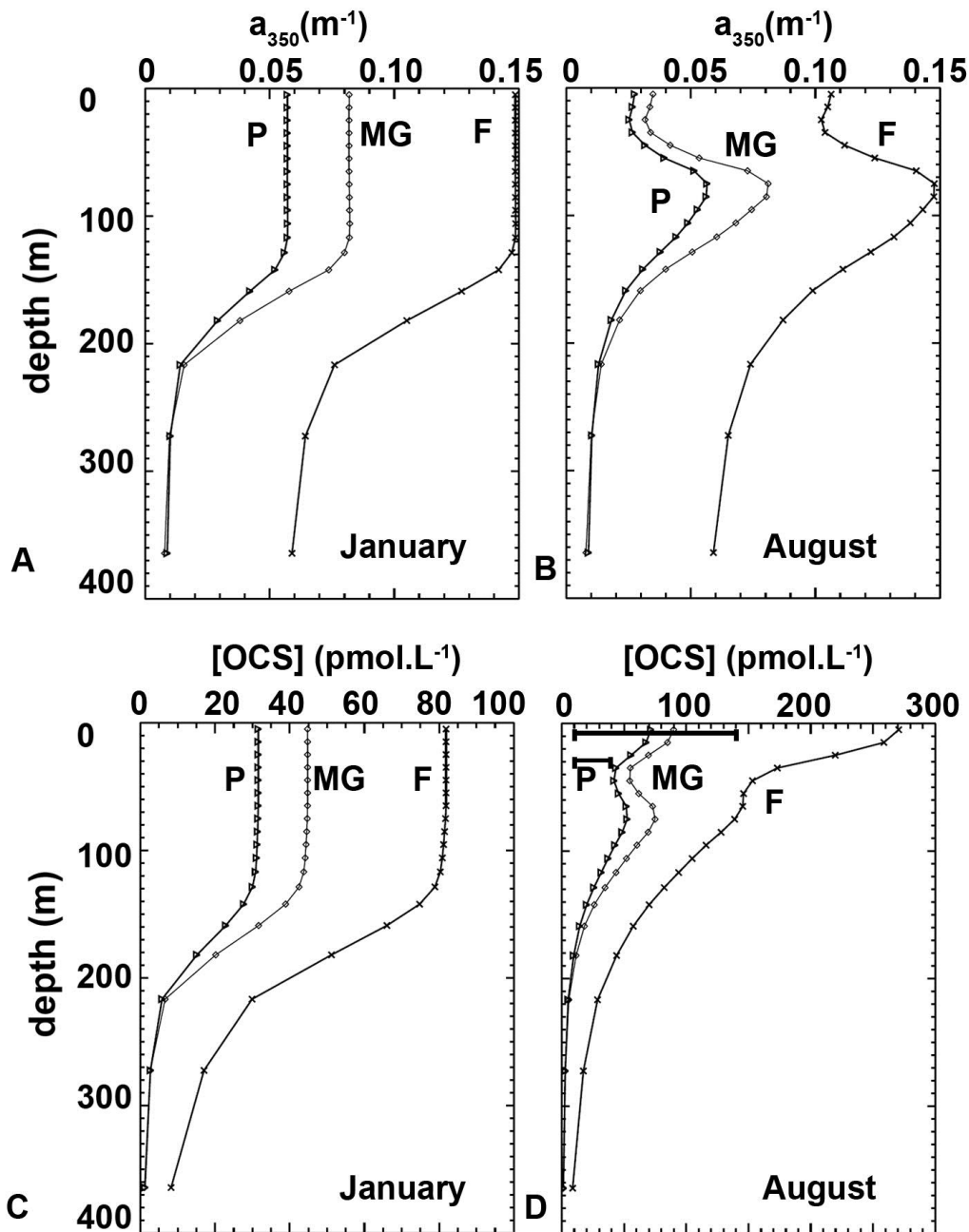
Figure 5: Monthly mean vertical profiles of a_{350} (top row) and OCS concentration (bottom row) in January (left column) and August (right column) simulated by NEMO-PISCES in a 1-D run at the Bermuda Atlantic Time Series (BATS) site. The thick lines on figure D cover the range between minimal and maximal values as measured by Cutter et al. (2004). The different a_{350} profile are calculated using the formulations of Morel and Gentili (2009) (MG, diamonds), Preiswerk et al. (2000) (P, triangles) or based on MODIS-*aqua* data (F, black line). Symbols used on OCS concentration profile on bottom row indicate which a_{350}-chlorophyll relation was used in the simulation.
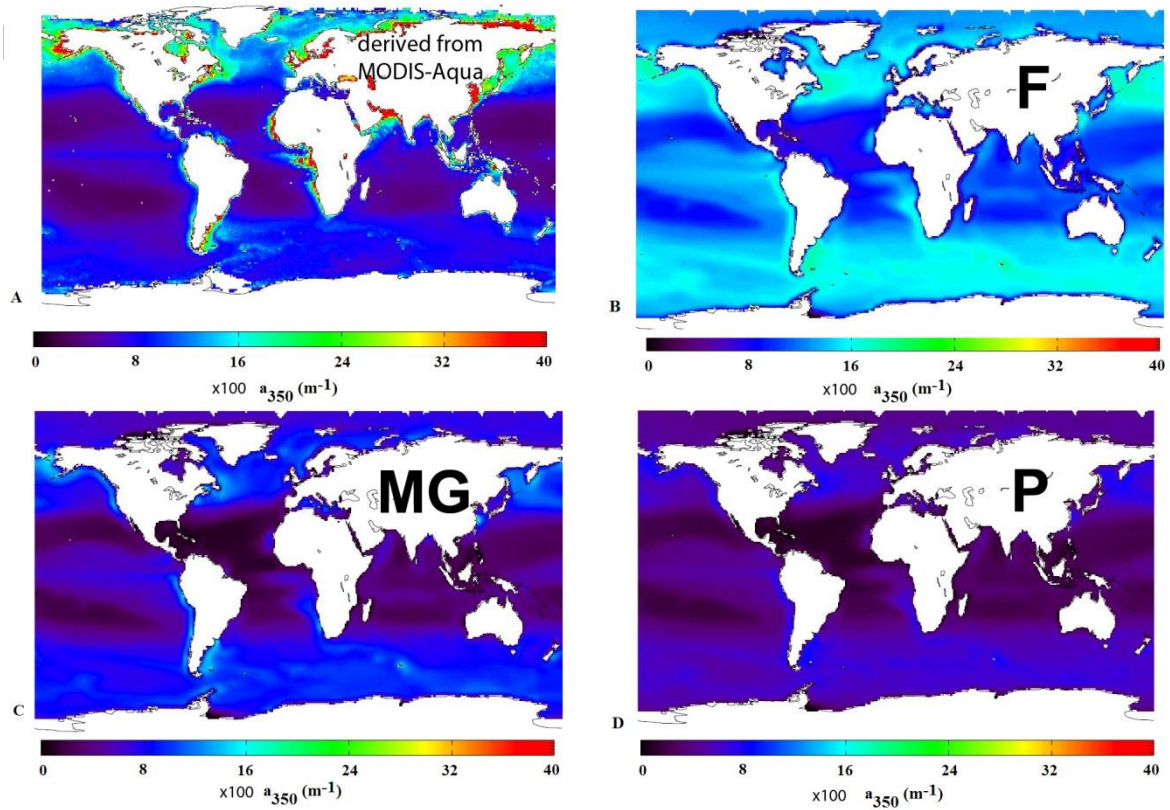
Figure 6: Comparison between annual mean surface absorption coefficient of CDOM at 350 nm: (A) retrieved from MODIS-*Aqua* satellites data, using SeaUV model (Fichot et al., 2008) and a_{320}/K_{d320} ratio from Fichot and Miller (2010) and a_{350} maps simulated with the NEMO-PISCES model using the relation described in Morel and Gentili (2009) (MG, panel C), Preiswerk et al. (2000) (P, panel D) or proposed in this work (F, panel B).
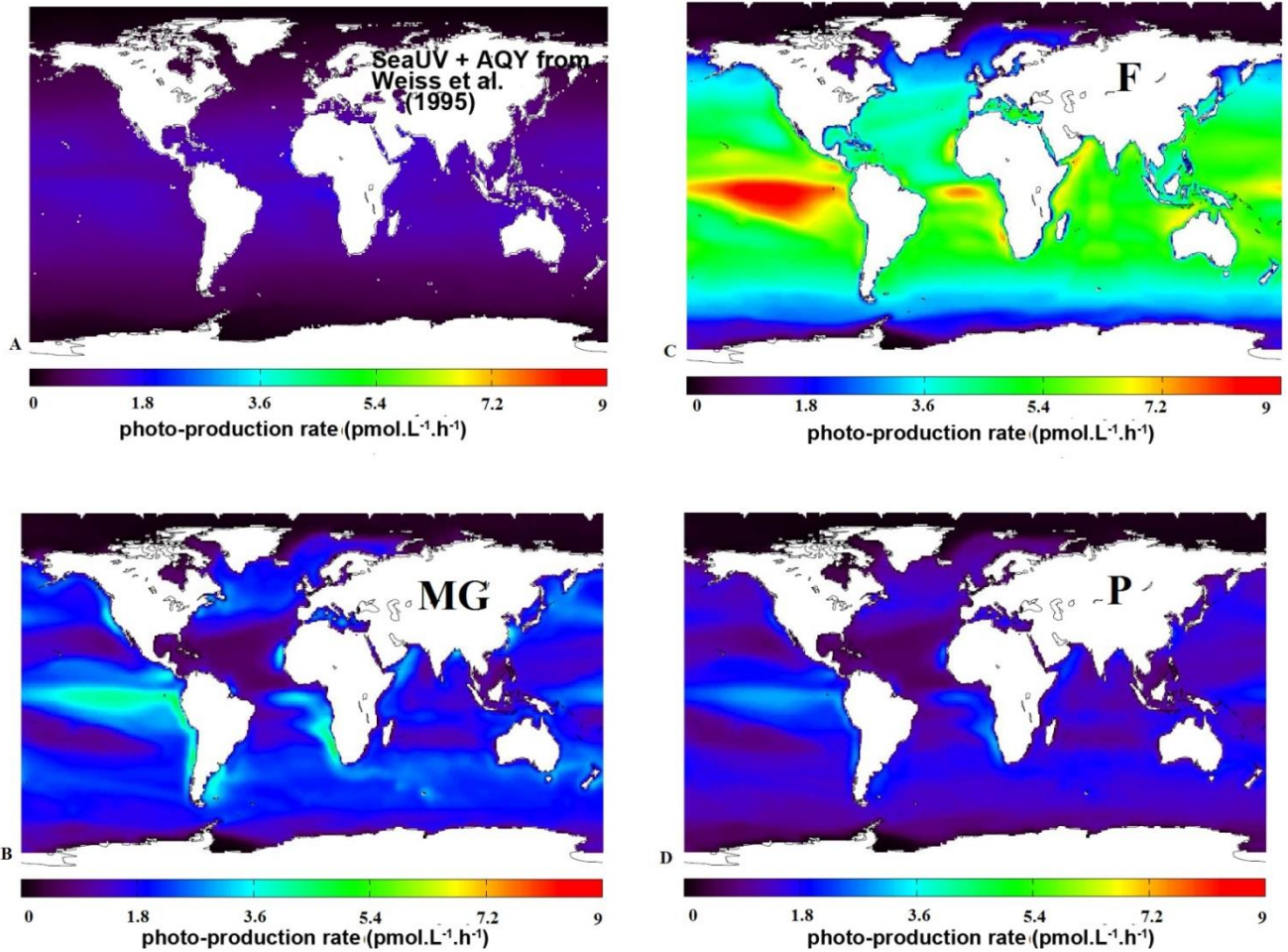
Figure 7: Annual mean photo-production rates integrated over the entire water column simulated with the photochemical model of Fichot and Miller (2010) and using the apparent quantum yield of Weiss et al (1995a) (panel A). Comparison with annual mean photo-production rates integrated over the entire water column simulated with the NEMO-PISCES model using a_{350} formulations from Morel and Gentili (2009) (panel C), Preiswerk et al. (2000) (panel D) or proposed in this study (panel B).

1
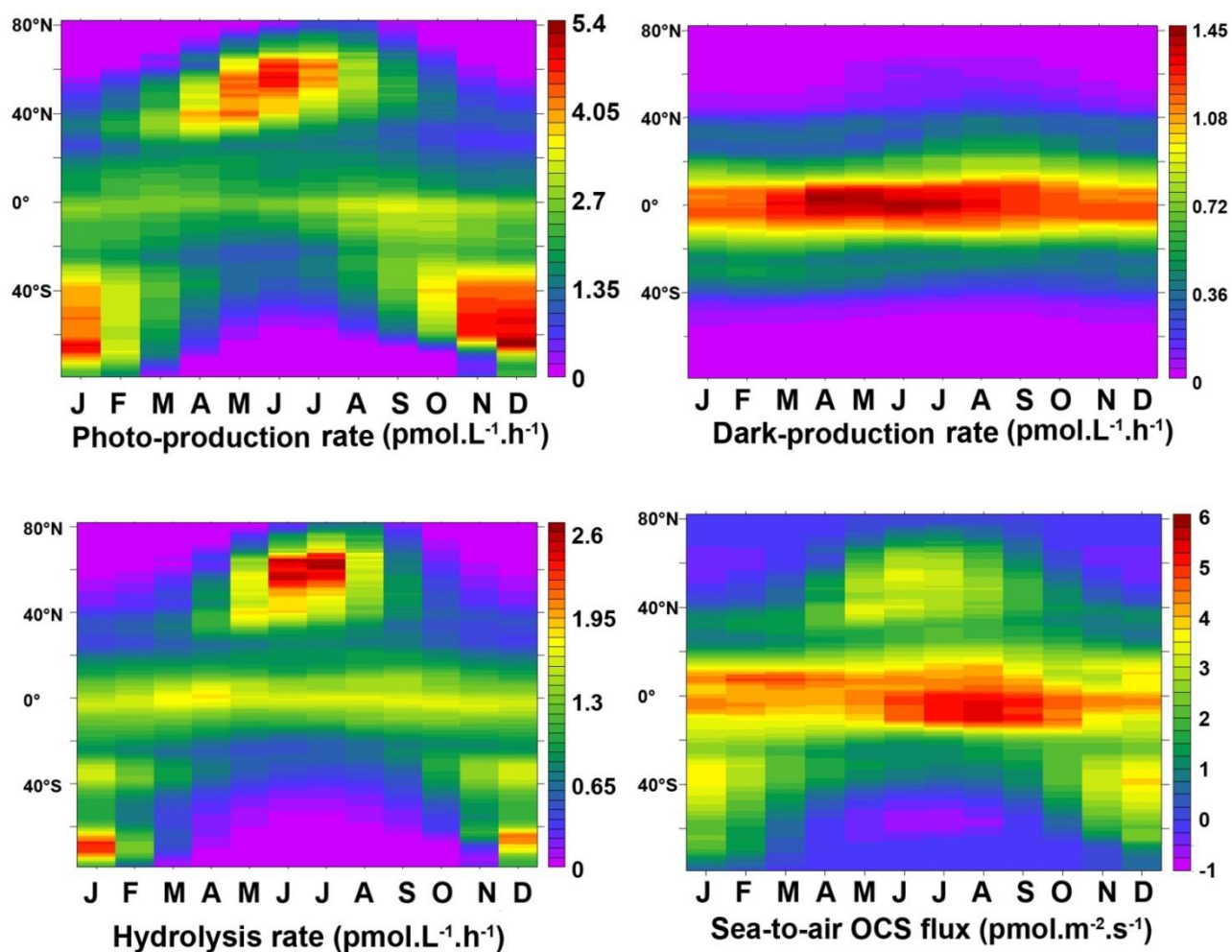
Figure 8: Latitude-time plots comparing relative importance of individual processes for OCS production (top row) and removal (bottom row) in NEMO-PISCES surface layer. Sea-air exchanges are displayed in bottom right panel are displayed with positive fluxes when OCS is outgassed towards the atmosphere. All runs were performed using Morel and Gentili (2009) formulation to calculate a_{350} and Elliott et al. (1989) formulation of hydrolysis constant.
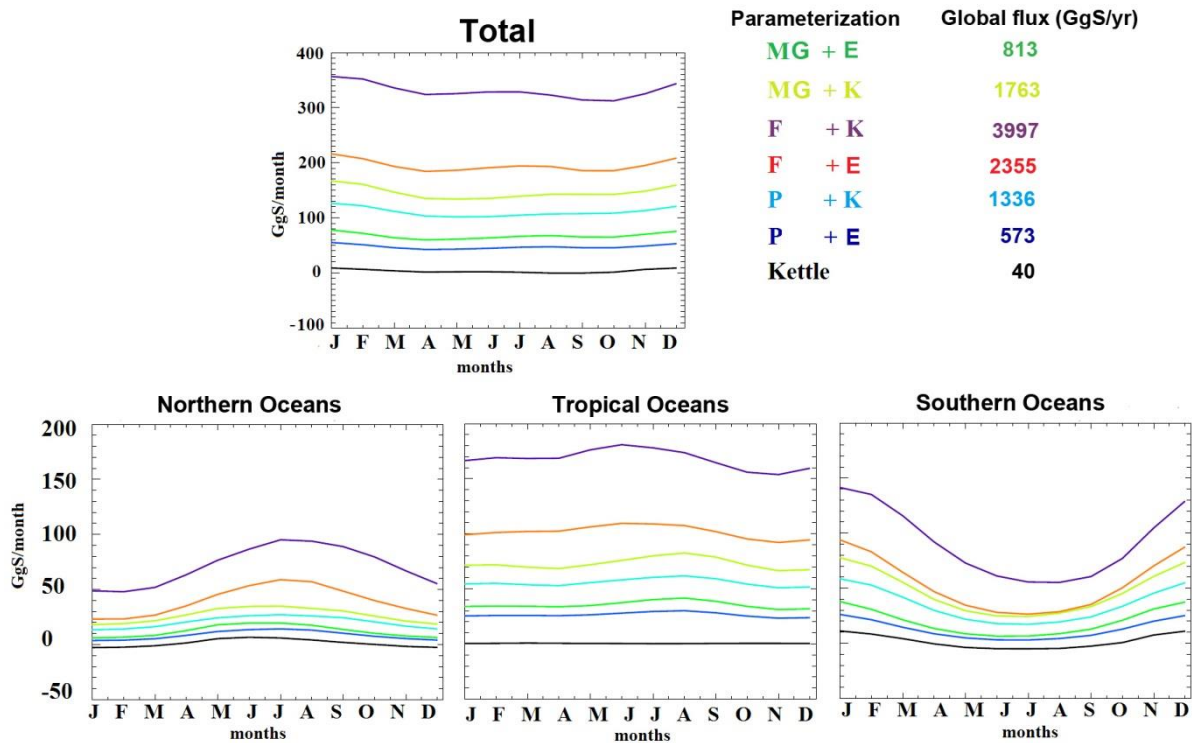
Figure 9: Global and regional monthly mean sea-air fluxes for 6 different parameterizations of the NEMO-PISCES model. Kettle et al. 2002 (black line) is shown as a reference. Each colored line represents a set of parameters: first name refers to the equation used to calculate the UV absorption coefficient of CDOM at 350 nm and the second name refers to the hydrolysis constant formulation. Global fluxes on top row, Northern Oceans (30°N-90°N, bottom left), Tropical region (30°S-30°N, bottom center), Southern Oceans (30°S-90°S, bottom right). F: a_{350} relation assembled in this study; MG: a_{350} relation from Morel and Gentili (2009); P: a_{350} relation from Preiswerk et al. (2000); E: hydrolysis constant from Elliott et al. (1989); K: hydrolysis constant from Kamyshny et al. (2003)
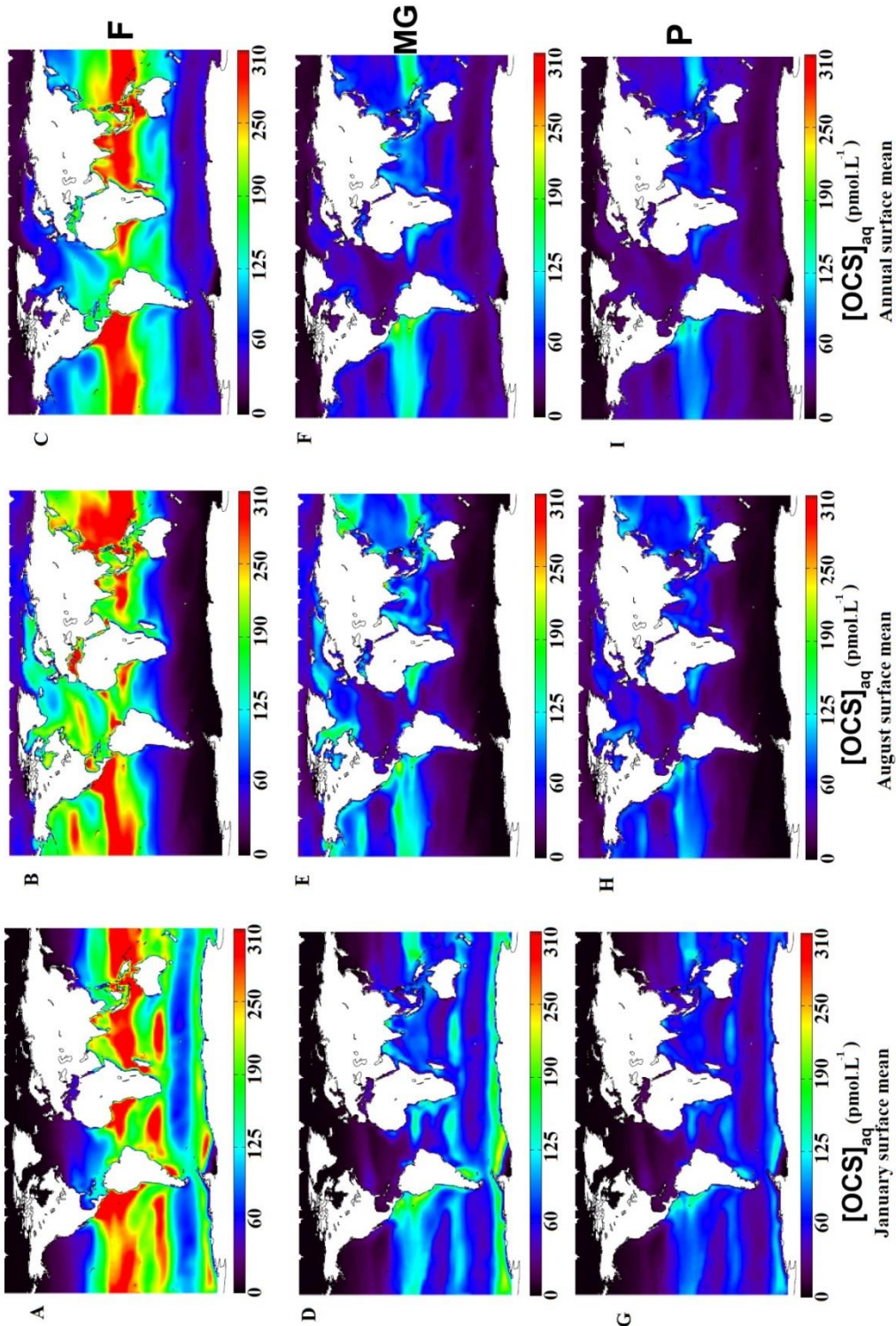
Figure 10: Monthly mean surface OCS concentrations for January (left column), August (central column) and annual mean (right column) simulated with NEMO-PISCES. The three simulations differ in the relationship used to calculate a_{350} from chlorophyll: MODIS *Aqua*-derived, proposed in this study (F, upper row), from Preiswerk et al. (2000)(P, central row) or Morel and Gentili (2009)(MG, lower row).

1

2

3

4

5

6

7

8   Table 1: Annual global photo-production of OCS in the entire water column simulated with

9   the NEMO-PISCES model (using the three different a_{350} formulations presented in this paper)

10 or with the photochemical model derived from Fichot and Miller (2010) (FM in the

11 table)(using two different apparent quantum yields estimates). F: a_{350} parameterization

12 assembled in this work; MG: a_{350} parameterization presented in Morel and Gentili (2009); P:

13 a_{350} parameterization presented in Preiswerk et al. (2000).

Parameterization used in the runs	Total photo-produced OCS in the entire water column (GgS yr^{-1})
NEMO-PISCES + F	4540
NEMO-PISCES + MG	1910
NEMO-PISCES + P	1390
FM + AQY from Weiss et al. (1995a)	876
FM + AQY from Zepp et al. (1994)	5500

14
15
16
17
18
19
20
21
22
23
24

1

2

3

4

5

6

7

8

9

Table 2: Yearly global OCS flux emitted from ocean to the atmosphere (in GgS yr^{-1}) depending on the different parameterizations presented in previous work and in this work. F: a_{350} parameterization presented in this work; MG: a_{350} parameterization presented in Morel and Gentili (2009); P: a_{350} parameterization presented in Preiswerk et al. (2000).

Study	Method		Annual flux (GgS yr^{-1})
Interpolation of observations			
Chin and Davis (1993)	sea surface OCS supersaturation ratios[a]		200 to 900
Watts (2000)	OCS surface concentration[b]		300*
Forward modeling			
	AQY/a$_{350}$	**hydrolysis constant**	
Kettle et al. (2002)[c]	AQY	Elliott et al., 1989	40**
Berry et al. (2013)[d]	from Kettle et al. (2002)	from Kettle et al. (2002)	736
This work standard run	a_{350} from MG	Elliott et al. (1989)	813

[a]sea surface OCS supersaturation ratios from opean oceans, upwelling zones and coastal regions

[b]OCS surface concentration from estuarine, coastal and open ocean environments

[c]Based on UV irradiance and apparent quantum yields from the literature. Lowest and highest boundaries of the estimates correspond to the lowest and highest AQY used.

[d]136 GgS yr^{-1} taken from Kettle upper estimate. Added source of 600 GgS yr^{-1} necessary to equilibrate the global budget.

* 100 GgS yr^{-1} from open ocean and 200 GgS yr^{-1} from coastal shores

1   ** uncertainty range: between -110 GgS yr^{-1} and +190 GgS yr^{-1}

2

3

4

5

6

7

8

9